AD NUMBER

AD486487

NEW LIMITATION CHANGE

TO

Approved for public release, distribution unlimited

FROM

Distribution authorized to U.S. Gov't. agencies and their contractors; Administrative/Operational Use; APR 1966. Other requests shall be referred to Air Force Materials Lab., AFSC, Wright-Patterson AFB, OH 45433.

AUTHORITY

AFWL ltr, 7 Dec 1972

486487

PROTON CORRELATION STUDIES

M. E. Wyatt
V. A. J. van Lint
E. G. Wikner

Special Nuclear Effects Laboratory
General Atomic Division, General Dynamics Corporation
San Diego, California

NOTICES

PROTON CORRELATION STUDIES

M. E. Wyatt
V. A. J. van Lint
E. G. Wikner

Special Nuclear Effects Laboratory
General Atomic Division, General Dynamics Corporation
San Diego, California

FOREWORD

This final report on proton correlation studies was prepared by the Special Nuclear Effects Laboratory, General Atomic Division, General Dynamics Corporation, San Diego, California, under Contract AF 33(615)-1715 with the Research and Technology Division, Wright-Patterson Air Force Base, Ohio. Mr. Robert Hickmott was the Air Force project monitor. The research reported herein was performed during the period 1 July 1964 through 31 January 1966. The General Atomic report number is GA-6953. The report was submitted March 4, 1966.

Publication of this report does not constitute Air Force approval of the reports findings or conclusions. It is published only for the exchange and stimulation of ideas.

RICHARD J. VOSSLER, Chief
High Energy Physics Branch
Materials Physics Division
AF Materials Laboratory

ii

ABSTRACT

The radiation effects of high-energy protons and electrons on germanium and silicon have been studied. The influence of the damage on the Hall effect and minority carrier lifetime produced by 1.5-, 2.3-, 5-, and 30-MeV electons is compared with that produced by 30- and 50-MeV protons. The experimental results are directly compared with the theoretical predictions of the damage. It is concluded that the higher-energy recoils resulting from the proton irradiations are more effective in producing damage than those resulting from the electron irradiations, based on the predictions of the total number of the defects that different types of particles are expected to produce. The reason for this may be that the higher-energy recoils produce displacements which are separated farther and thereby influence the measured properties in a different manner.

Complexities in correlating proton and electron damage which arise from the influence of impurities and defect motion during irradiation are discussed. A proton simulation based on an admixture of electrons and reactor neutrons is discussed theoretically.

CONTENTS

Tables

SECTION I

INTRODUCTION

Radiation produces permanent damage in semiconductor materials by displacing the lattice atoms, which in turn may form electrically active defect structures in the lattice. These defects could change the important electrical properties of the material, such as the conductivity, carrier mobility, number of carriers, and the minority carrier lifetime, and thus the characteristics of a device built of these materials are altered as the result of irradiation.

A spectrum of electron energy irradiations, 1.5, 2.3, 5, and 30 MeV, of semiconductor materials are compared with those of 30-MeV and 50-MeV proton irradiations in order to determine whether proton damage can be simulated by electron damage. The effect of proton damage, of course, is important in space applications, and it is of interest whether the effect of this damage is the same as for electron-produced damage, primarily because electrons are a more available radiation source. The experimental results are directly compared with theoretical predictions of the damage produced by several types of irradiations. From a theoretical standpoint, a comparison of 30-MeV electrons with protons is of primary interest as they are most likely to be commensurate. Also, comparisons of the experimental results are made with theoretical predictions for electrons of 1.5-, 2.3-, and 5-MeV energy and for protons of 50-MeV energy. These low-energy electrons provide a check on the lower limit of electron energies capable of simulating protons and the 50-MeV protons provide a check on the effect of the larger displacement clusters.

The materials irradiated were chosen to cover a spectrum of semiconductor materials. The twelve chosen consisted of 0.5-ohm-cm and

1

10-ohm-cm samples of boron-doped p-type silicon, phosphorus-doped n-type silicon, gallium-doped p-type germanium, and arsenic-doped n-type germanium. The silicon samples consisted of both floating-zone refined and quartz-crucible pulled materials to check the effects of oxygen content, whereas all of the germanium samples were quartz-crucible pulled.

The physical properties chosen for measurement were those that are most intimately associated with device operation and also sensitive to radiation: the carrier concentration and carrier lifetime. The carrier concentration is presented as a removal rate, or the average number of carriers per cubic centimeter removed per incident particle per square centimeter, and the carrier lifetime is presented as a rate of change of inverse lifetime with incident particle flux. Post-irradiation annealing experiments were made in an attempt to identify by inference some of the properties of the defect responsible for the damage.

A unitary positive correlation between irradiations with different incident particles requires a constant ratio of damage rates across a spectrum of materials and damage types. Any properties inferred about the defects responsible for the damage should also match. However, a lesser degree of correlation with different irradiations would still be useful in predicting damage rates.

SECTION II

THEORETICAL CORRELATION OF DISPLACEMENT EFFECTS
FROM PROTONS, ELECTRONS, AND NEUTRONS
IN SILICON AND GERMANIUM

2.1. INTRODUCTION

A complete theory of displacement radiation effects would describe the sequence of events occurring to produce lattice defects and would relate the character of the resulting defects to change in macroscopic physical properties of the irradiated material. The sequence of events described would include:

1. Collisions between the incident radiation and the target to produce recoil atoms.

2. Motion of recoil atoms through the lattice to produce subsequent generations of secondary displacements, leading eventually to the dissipation of the kinetic energy of the recoil atoms and to the establishment of thermal equipartition of kinetic energy.

3. Subsequent thermal-activated motion of defects to form secondary defect structures which are stable at the sample temperature.

4. The relation between the microscopic structure of the defects and the macroscopic physical properties, which are measured.

It is obvious that such a complete theory is not available, and its lack might cause one to despair of establishing a sound theoretical relation between primary irradiation and physical property changes. The most imposing obstacle appears to be a description of thermal motion and secondary defect formation, particularly as influenced by impurities and defects already present in the crystal before irradiation. It is well known

3

that impurities which have no significant effect on the important electrical properties of a semiconductor may influence strongly its irradiation response. Interstitial oxygen in silicon is a well-known example.

Fortunately, in attempting to establish not the absolute magnitude of the damage but only the correlation between damage produced by different irradiating particles, it is possible to be less demanding of the theory. Specifically, it is obvious that if each of two irradiations produces the same concentration and energy spectrum of primary recoil atoms, the resulting damage must also be the same. Even this requirement may be too severe. A high-energy recoil atom tends to lose most of its energy by a large number of collisions, in each of which the fractional energy loss is small.[1] Moreover, the higher-energy recoils (>100 keV for silicon) tend to lose much of their energy by ionization until the residual energy is significantly lower. Hence, as far as the displacement structure is concerned, there is not much difference between a 100-keV and a 200-keV silicon recoil atom.

If it is also assumed that the physical properties measured are sensitive to change in lattice structure over regions small compared to the range of a high-energy recoil atom, it can be asserted that the damage should be a function only of the total energy expended in displacement production (recoil energy minus ionization loss). At a cursory glance, the secondary recoils produced along a high-energy primary recoil track have an energy not strongly dependent on the primary recoil energy, and hence their number increases with increasing primary energy, but the character of the damage may not change.

This discussion suggests that there is an excellent chance of establishing a correlation between two irradiations, provided two conditions are met:

1. The number and energy spectrum of lower-energy recoils must be the same, and

2. The amount of energy expended in displacement production by high-energy recoils must be the same.

4

The transition point between low- and high-energy recoils is not known, but intuitively it should correspond to displacement clusters containing at least tens of displacement recoils (i.e., primary recoil energy is >1 keV).

The purpose of the following discussion is to examine in detail the energy distribution of primary recoils resulting from electron, proton, and neutron collisions and to evaluate the possibility of correlating electron and proton irradiations. The conclusion to be noted is that with an appropriate scaling factor for the Rutherford cross section, high-energy electrons and protons satisfy the first condition above, but that for this scaling factor influence, the total displacement energy imparted by protons via high-energy recoils is larger than for electrons. This extra portion could be adequately reproduced by adding a reactor neutron irradiation to the electron bombardment.

Protons and electrons both interact with an atom at low-energy transfers primarily through Rutherford scattering, and the scattering cross sections have the same dependence on energy transfer for both at the low end of the primary recoil energy spectra. For protons at higher primary recoil energies, nuclear elastic scattering becomes important, and the scattering cross section results in a dip and then a peak in comparison with the shape of the Rutherford scattering. Further oscillations in the cross section are generally less important as these occur at high-enough primary recoil energies that most of the energy of the recoil is lost through electronic collisions and only a small part goes into displacing atoms. The nuclear elastic effect may be important at proton energies as low as 10 MeV and must be taken into account whenever proton damage rates are considered.

The low-energy part of the proton recoil spectrum may be simulated by electrons by choosing the electron energy such that the lessening of the electron scattering cross section at high primary recoil energies due to relativistic effects approximates the first dip in the proton cross section. The following peak in the proton cross section may be simulated by reactor neutrons which give little contribution at low primary recoil energies but

5

produce a peak at higher energies similar to that of the protons. The quantities of electrons and reactor neutrons can be mixed to give the same total number of displacements as protons and with a primary recoil atom energy spectrum similar in shape up to much higher energies than with electrons alone.

Nuclear inelastic scattering was neglected in calculating the proton damage rates and it is possible that the displacement production is under-estimated by up to 50 percent in germanium at 50 MeV. The effect is less effective for silicon and lower incident proton energies but still may be as much as 25 percent in silicon at 30 MeV.

2.2. PRIMARY RECOIL IONIZATION ENERGY LOSS

As the energy of a primary recoil atom from a scattered particle is increased, a smaller proportion of its energy will go into displacement collisions, a greater proportion of its energy being lost through ionizing collisions with orbital electrons. The fraction of energy lost in elastic or atomic collisions has been computed by Lindhard,[2] assuming a Thomas-Fermi potential for atomic scattering and a velocity-dependent electronic stopping power. The results of Lindhard's calculations for silicon and germanium are shown in Fig. 1 as the fraction, f, of the primary recoil energy that goes into displacement-type collisions. This fraction is used in the calculation for the number of displacements from a primary recoil atom instead of the more usual arbitrary cut-off energy beyond which a recoil atom is assumed to produce no displacements.

2.3. RUTHERFORD SCATTERING

The mechanism by which charged particles impart energy to a lattice atom is, neglecting nuclear forces and screening by orbital electrons, Rutherford or Coulomb scattering[3] with a differential cross section of

$$\frac{d\sigma_R}{dT} = \frac{nb^2}{4} \cdot \frac{T_m}{T^2} \, ,$$

6
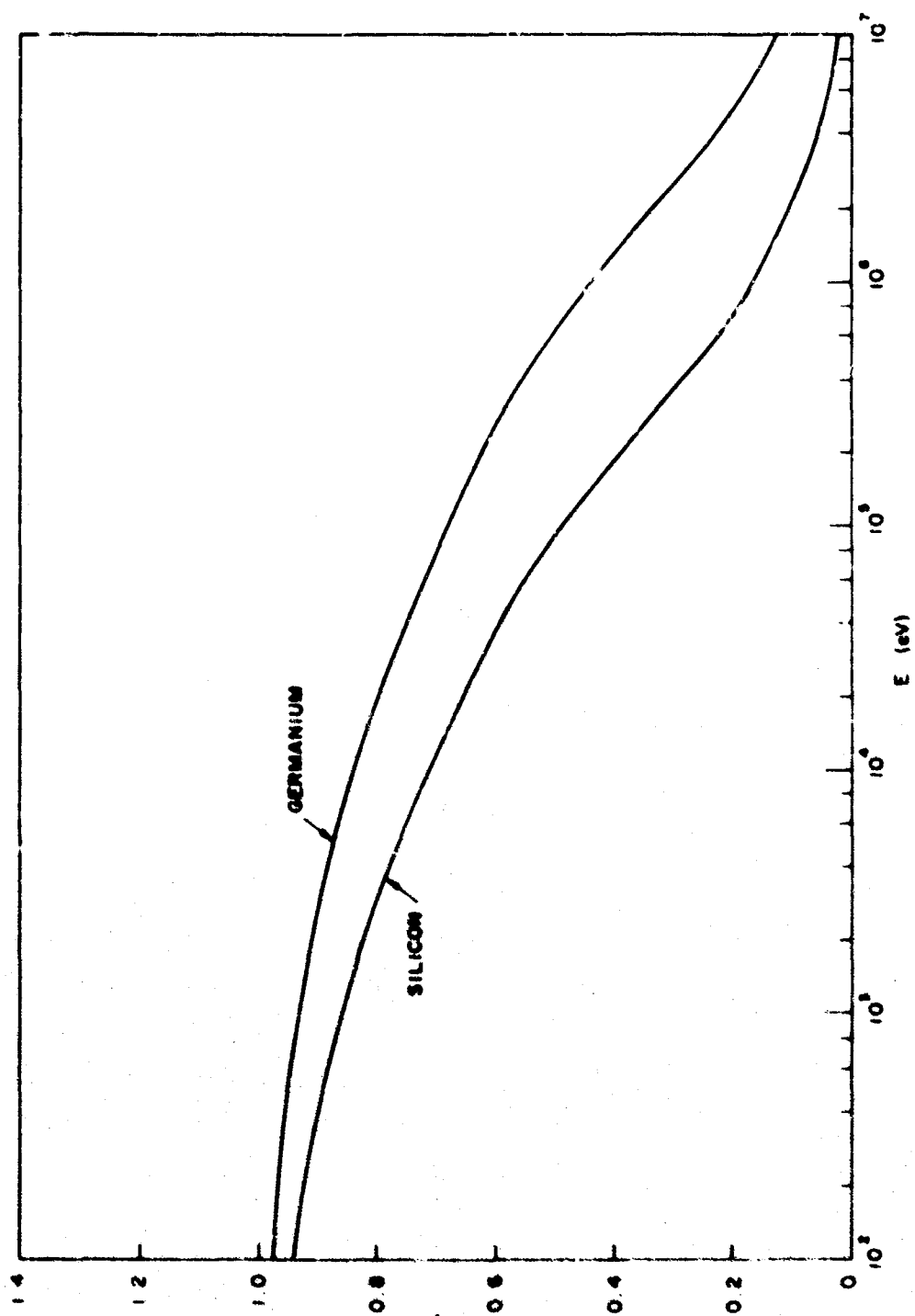
Figure 1. Fraction of primary recoil energy lost in displacement-type collisions

7

where T is the recoil atom's kinetic energy, T_m is the maximum energy transfer, and b is the classical distance of closest approach in a head-on collision.

At recoil energies much greater than the displacement energy, T_d, the number of displaced atoms per primary recoil is linearly related to the recoil energy and may be taken as $0.5\ T/T_d$. Using the number of displaced atoms produced as the physically significant quantity, the number of displacements produced by primary recoils between energies T_1 and T_2 is

$$N_d = \int_{T_1}^{T_2} \frac{T}{2T_d} \frac{d\sigma_R}{dT} dT = \frac{\pi b^2}{8} \frac{T_m}{T_d} \ln \frac{T_2}{T_1} \ ,$$

showing that each logarithmic energy interval contributes equally to the number of displacements. This suggests a comparison between protons and electrons of the ratio of the true to Rutherford cross section versus the logarithm of the primary recoil energy.

2.4. NUCLEAR ELASTIC SCATTERING

Protons and neutrons both undergo nuclear elastic scattering in the force field of the target nucleus. This scattering is fairly well understood in terms of the optical model of the nucleus,[4-7] and a number of experiments[8-13] have been performed to measure the scattering cross section. In fact, extensive measurements have been made of the scattering of protons and neutrons on aluminum and copper, whereas few measurements have been made on either silicon or germanium. Since the experimental measurements and the predictions of the optical model both show a slow variation of the cross sections as a function of atomic number, the cross sections for aluminum and copper have been used for silicon and germanium. The scattering cross sections for 30-MeV protons on aluminum, silicon, and phosphorous and on copper and gallium (taken from Ref. 8), are shown in Fig. 2 to illustrate the slow variation between adjacent elements. The ratio of the measured to Rutherford cross section is plotted

8
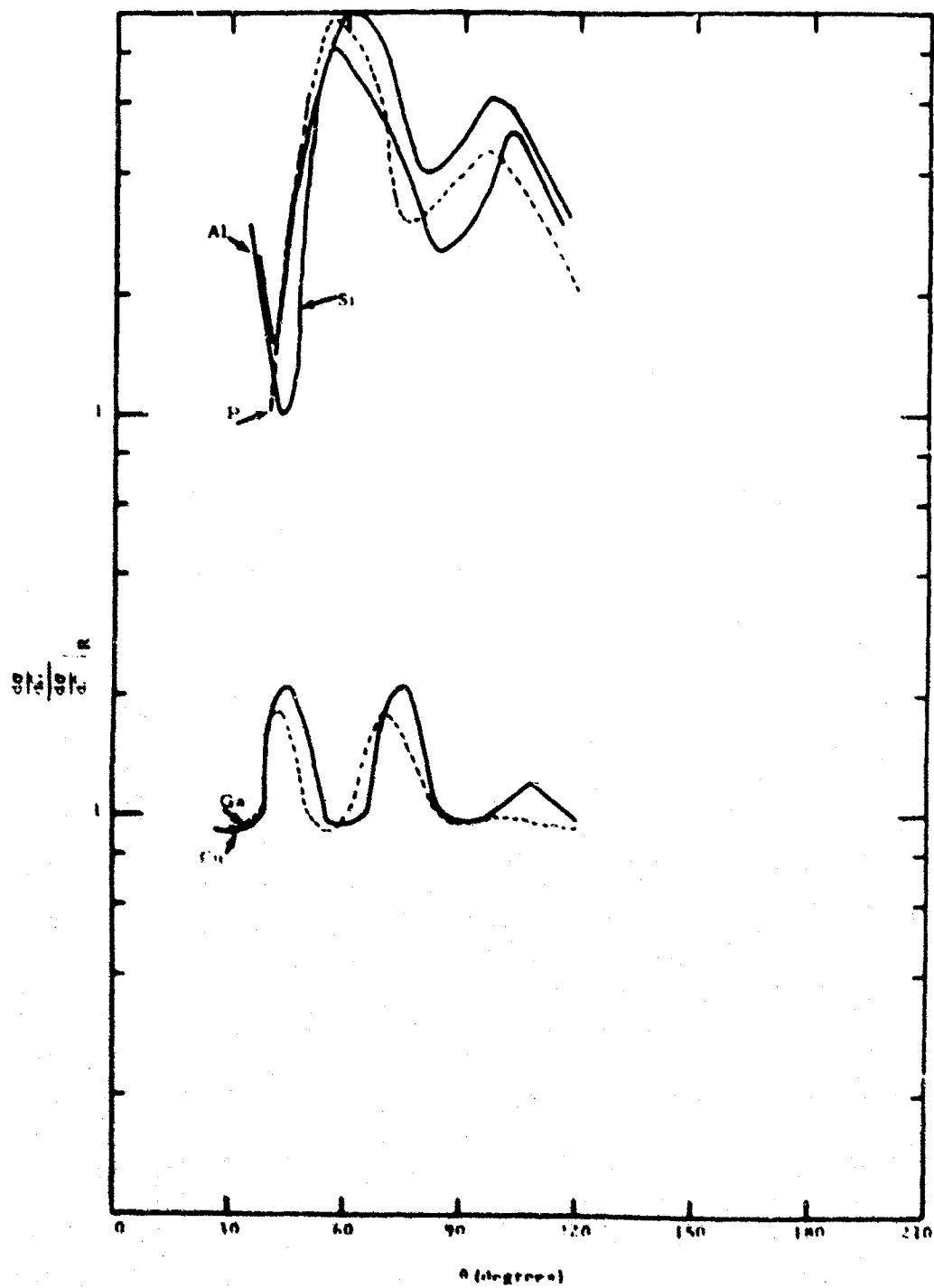
Figure 2. Ratio of measured elastic scattering cross section to the calculated Rutherford cross section as a function of center-of-mass scattering angle for 30-MeV protons

9

to accentuate the nuclear elastic effect and to eliminate the elemental dependence of the Rutherford cross section, which all of the cross sections approach at low energy transfers.

2.5 PROTON DAMAGE

For incident protons, the cross section, N_{dp}, for producing displacements from primary recoils between energies T_1 and T_2 is

$$N_{dp} = \int_{T_1}^{T_2} \frac{T}{2T_d} \frac{d\sigma}{d\sigma_R}(T) f(T) \frac{d\sigma_R}{dT} dT , \qquad (1)$$

where $d\sigma/d\sigma_R$ is the ratio of the measured to Rutherford cross section, and f is the fraction of the recoil energy lost in displacement-type collisions.

The Rutherford cross section for nonrelativistic protons is

$$\frac{d\sigma_R}{dT} = \frac{\pi b^2}{4} \frac{T_m}{T^2} = \frac{\pi Z^2 e_0^4}{A E_0 T^2} ,$$

where A and Z are the atomic weight and atomic number, respectively, of the target atom, E_0 is the incident proton energy, e_0 is the electronic charge,

$$b = \frac{Z e^2 \left(1 + \frac{1}{A}\right)}{E_0} \quad \text{and} \quad T_m = \frac{4}{A}\left(1 + \frac{1}{A}\right)^{-2} E_0 .$$

The ratio of the measured elastic scattering cross section to the Rutherford cross section for aluminum and copper is plotted in Figs. 3 and 4, respectively, for a number of incident proton energies. (The references from which these are taken are noted on the figures.) Because of the smooth variation in the cross section with incident proton energy, an interpolation was performed between 40 and 57 MeV to give the 50-MeV cross section. The cross sections used at 30 and 50 MeV for silicon and germanium, together with the function f, are plotted in Figs. 5 and 6, respectively.

10
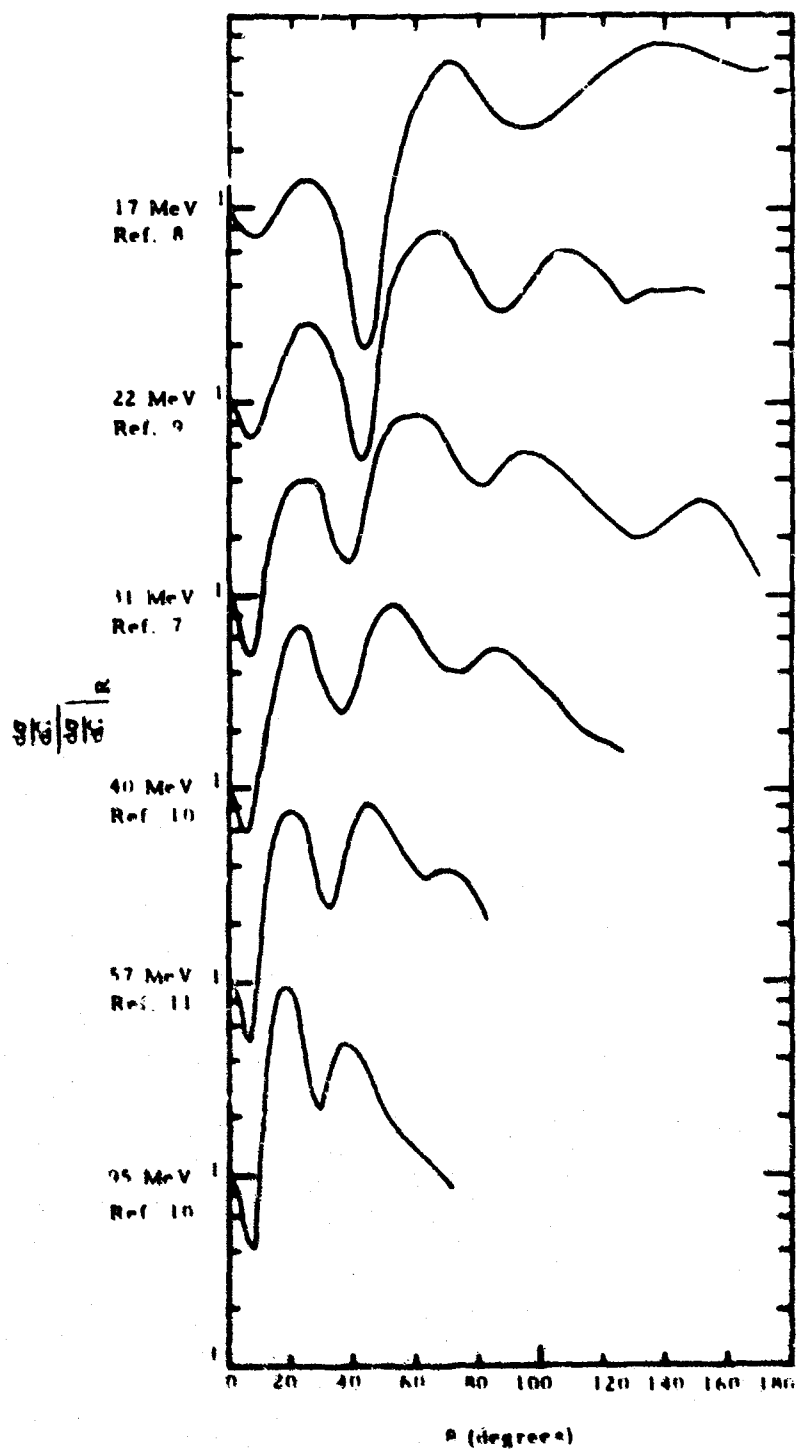
Figure 3. Ratio of measured elastic scattering cross section to the calculated Rutherford scattering cross section vs center-of-mass scattering angle for aluminum

11
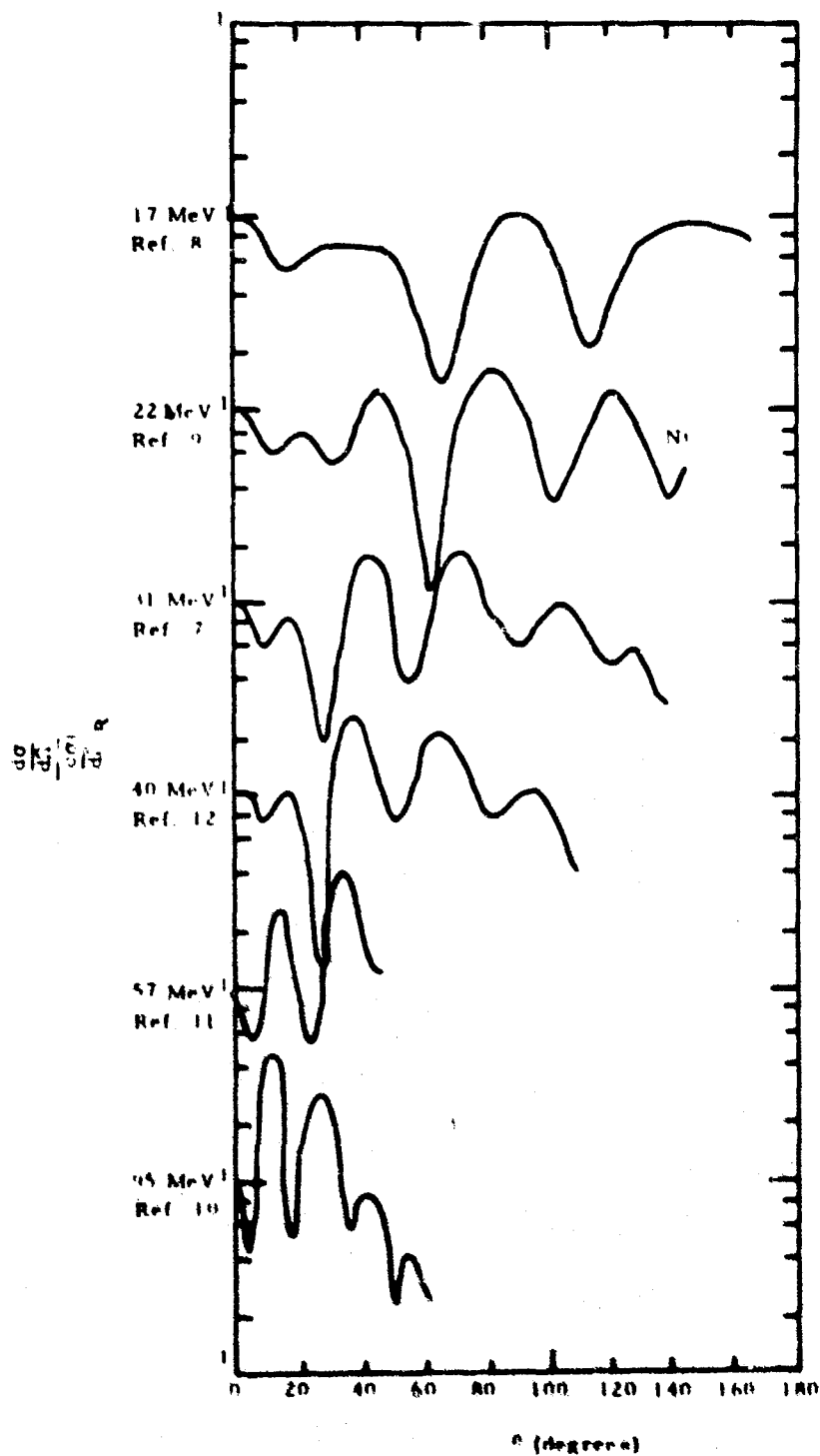
Figure 4. Ratio of measured elastic scattering cross section to the calculated Rutherford scattering cross section vs center-of-mass scattering angle for copper
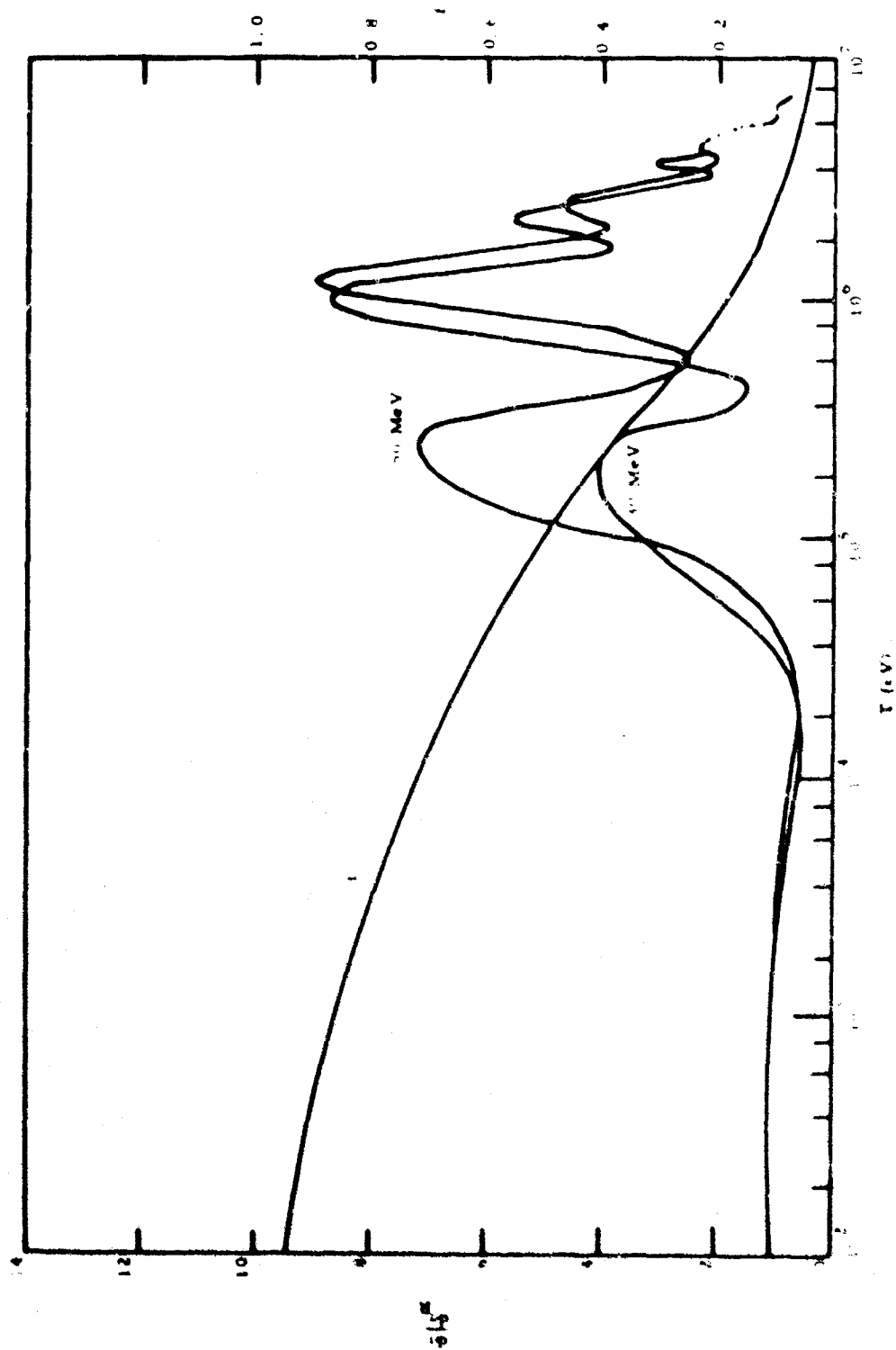
Figure 5. Ratio of measured elastic scattering cross section to the calculated Rutherford scattering cross section vs recoil energy for silicon
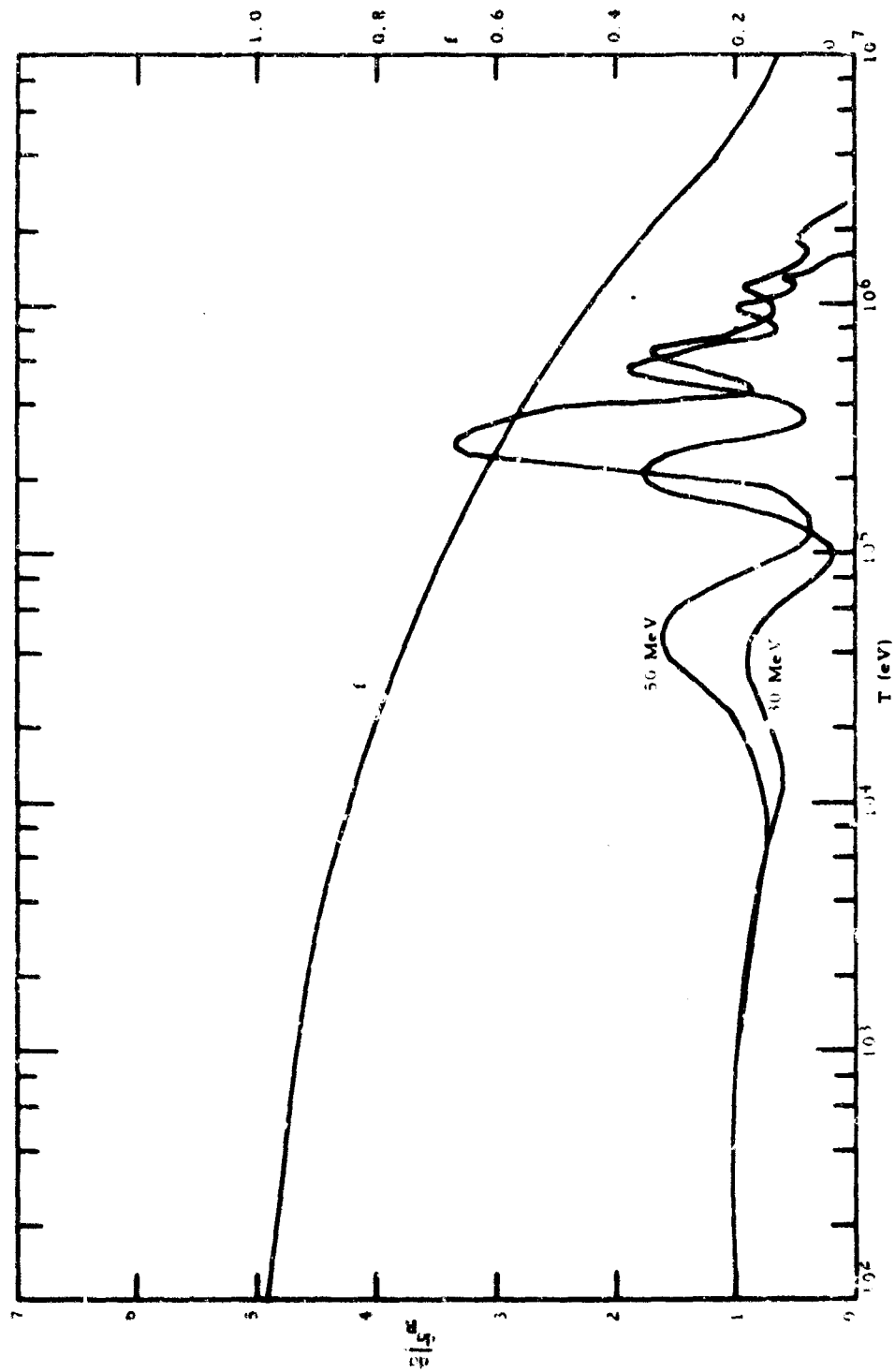
Figure 6. Ratio of measured elastic scattering cross section to the calculated Rutherford scattering cross section vs recoil energy for germanium

14

For the purposes of numerical calculation, the average value of $d\sigma/d\sigma_R$ and f are taken over the interval ΔT_i about T_i. On integration, this reduces Eq. (1) to

$$N_{dp}(T_i) = \overline{\frac{d\sigma}{d\sigma_R}}\bigg|_{T_i} \overline{f}_{T_i} \frac{\pi Z^2 e_0^4}{2A E_0 T_d} \ln \frac{T_{i+1/2}}{T_{i-1/2}} ,$$

where

$$T_{i+1/2} = T_{i-1/2} + \Delta T_i \quad \text{and} \quad T_i = [T_{i+1/2}^2 + T_{i-1/2}^2]^{1/2}$$

to give the aforementioned logarithmic energy intervals. Five intervals were taken per decade, resulting in

$$\ln (T_{i+1/2}/T_{i-1/2}) = 0.462 .$$

The cross section for producing displacements from recoil atoms with energy in the interval ΔT_i about T_i is then given by

$$N_{dp}(T_i) = 0.231 \frac{\pi Z^2 e_0^4}{A E_0 T_d} \overline{\frac{d\sigma}{d\sigma_R}}\bigg|_{T_i} \overline{f}_{T_i} \tag{2}$$

and the total cross section for displacements produced by recoil atoms with energy from T_d to T_i, $N_{dpt}(T_i)$, is

$$N_{dpt}(T_i) = 0.231 \frac{\pi Z^2 e_0^4}{A E_0 T_d} \sum_{T_d}^{T_i} \overline{\frac{d\sigma}{d\sigma_R}}\bigg|_{T_i} \overline{f}_{T_i} . \tag{3}$$

Equations (2) and (3) are plotted for silicon in Figs. 7 and 8, respectively, and are plotted for germanium in Figs. 9 and 10, respectively, for protons of 30- and 50-MeV incident energy. These figures are plotted in units of $0.231 \pi Z^2 e_0^4/A E_0$ for direct comparison with the recoil spectra of other types of scattering. Also plotted in Figs. 8 and 10 are the results

15
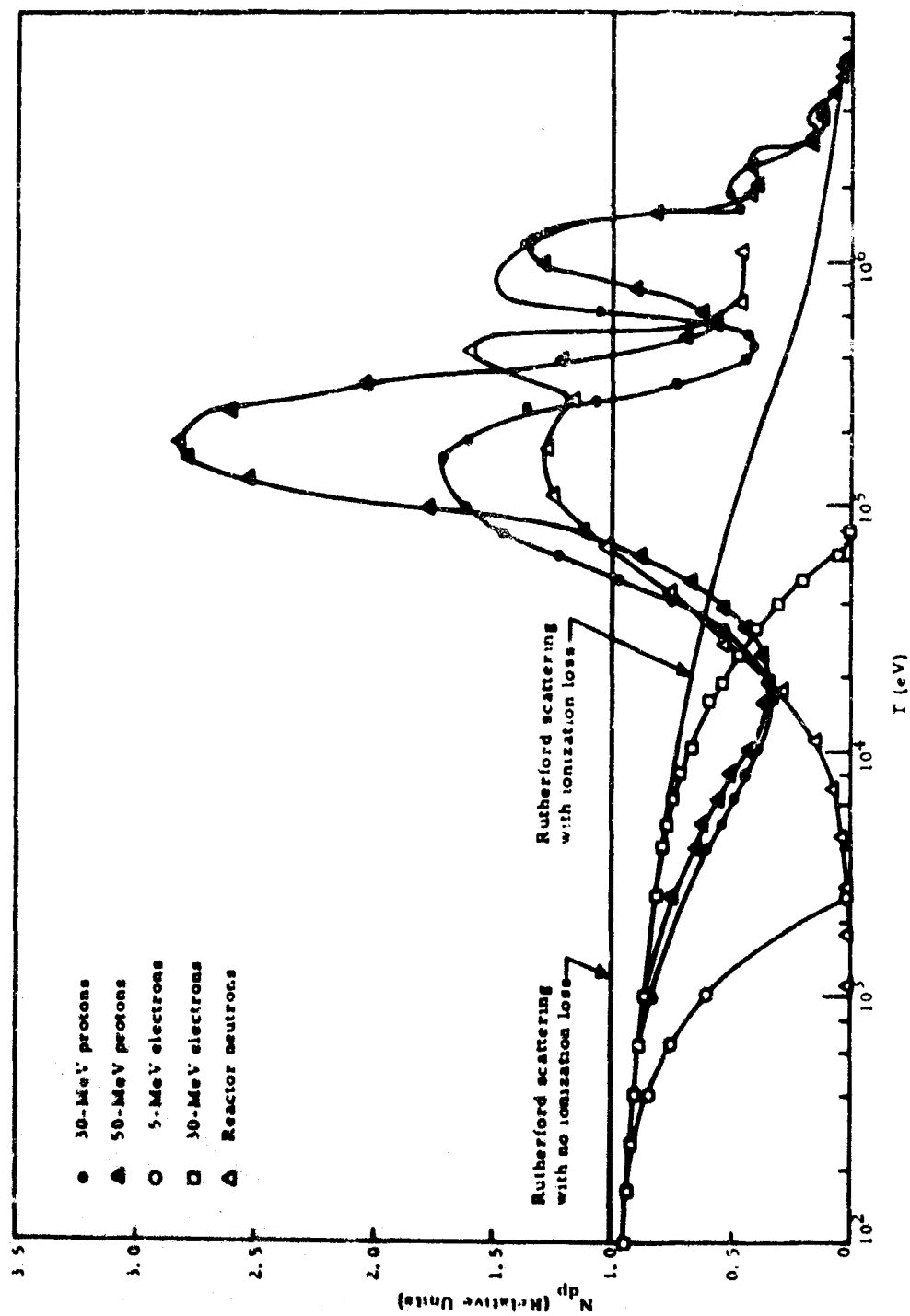
Figure 7. The number of atoms displaced by recoil atoms with energy ΔT about T vs T for silicon
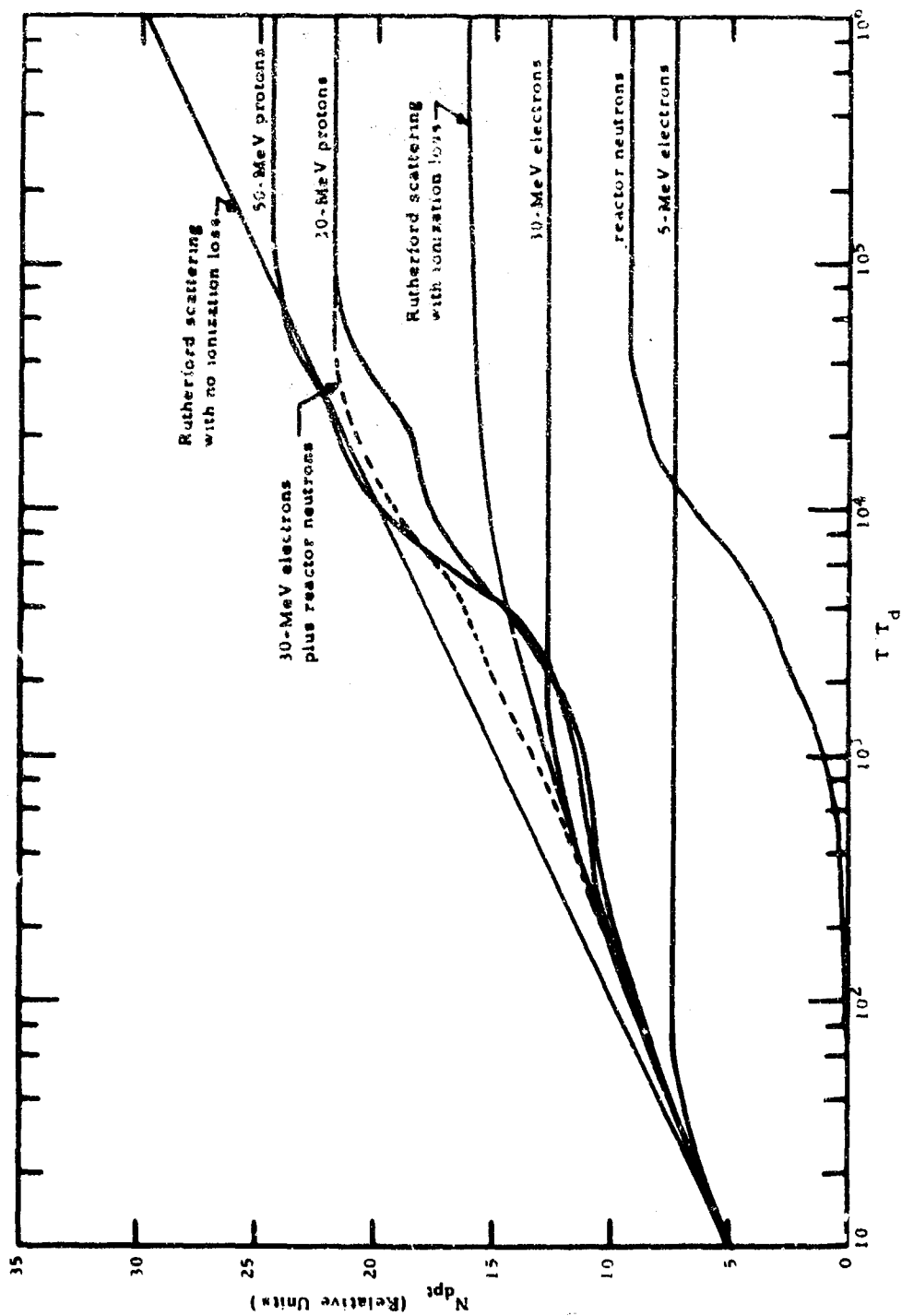
Figure 8. Total number of displaced atoms produced by recoil atoms with energy from T_d to T vs T/T_d for silicon

17
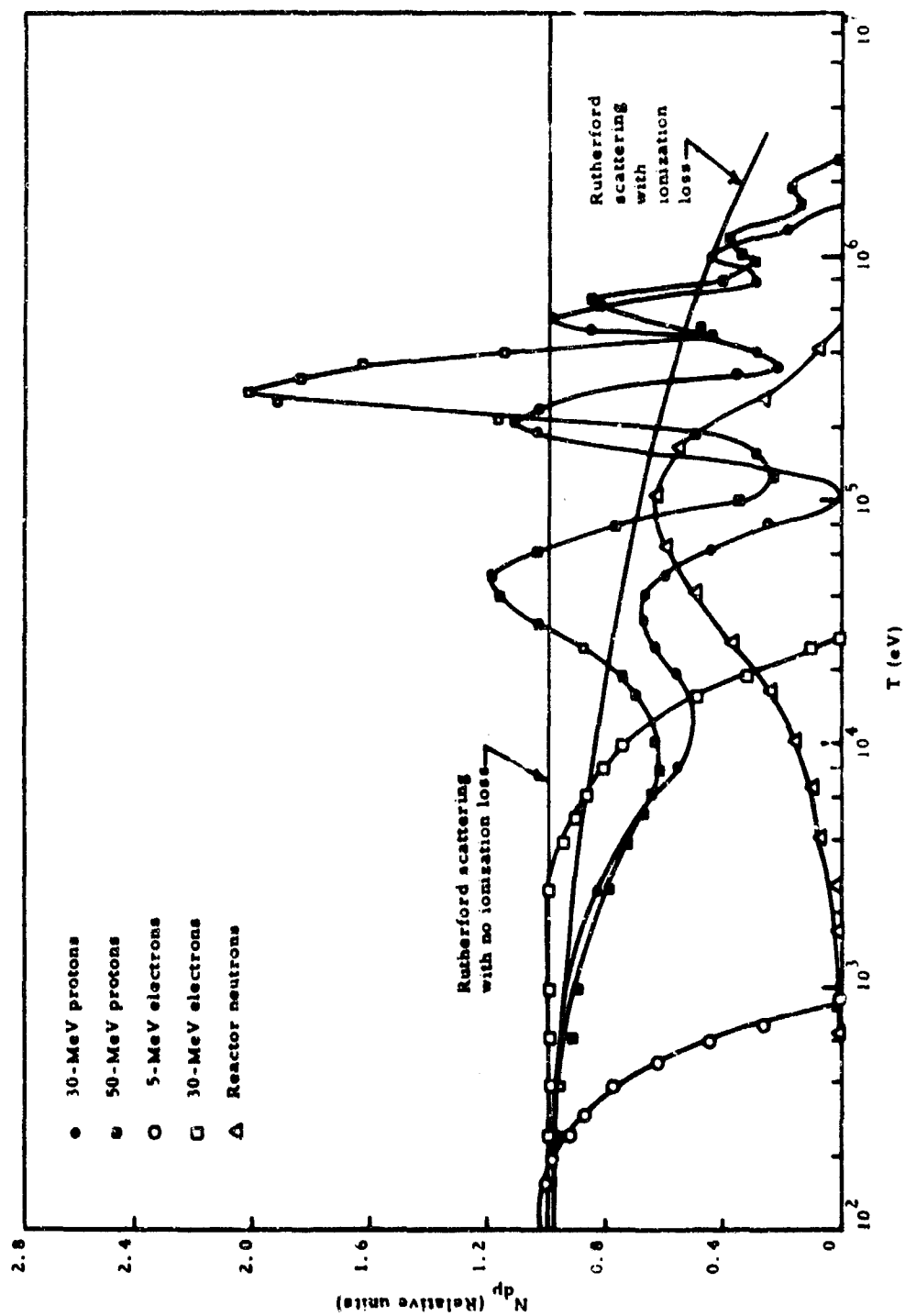
Figure 9. The number of atoms displaced by recoil atoms with energy ΔT about T vs T for germanium

18
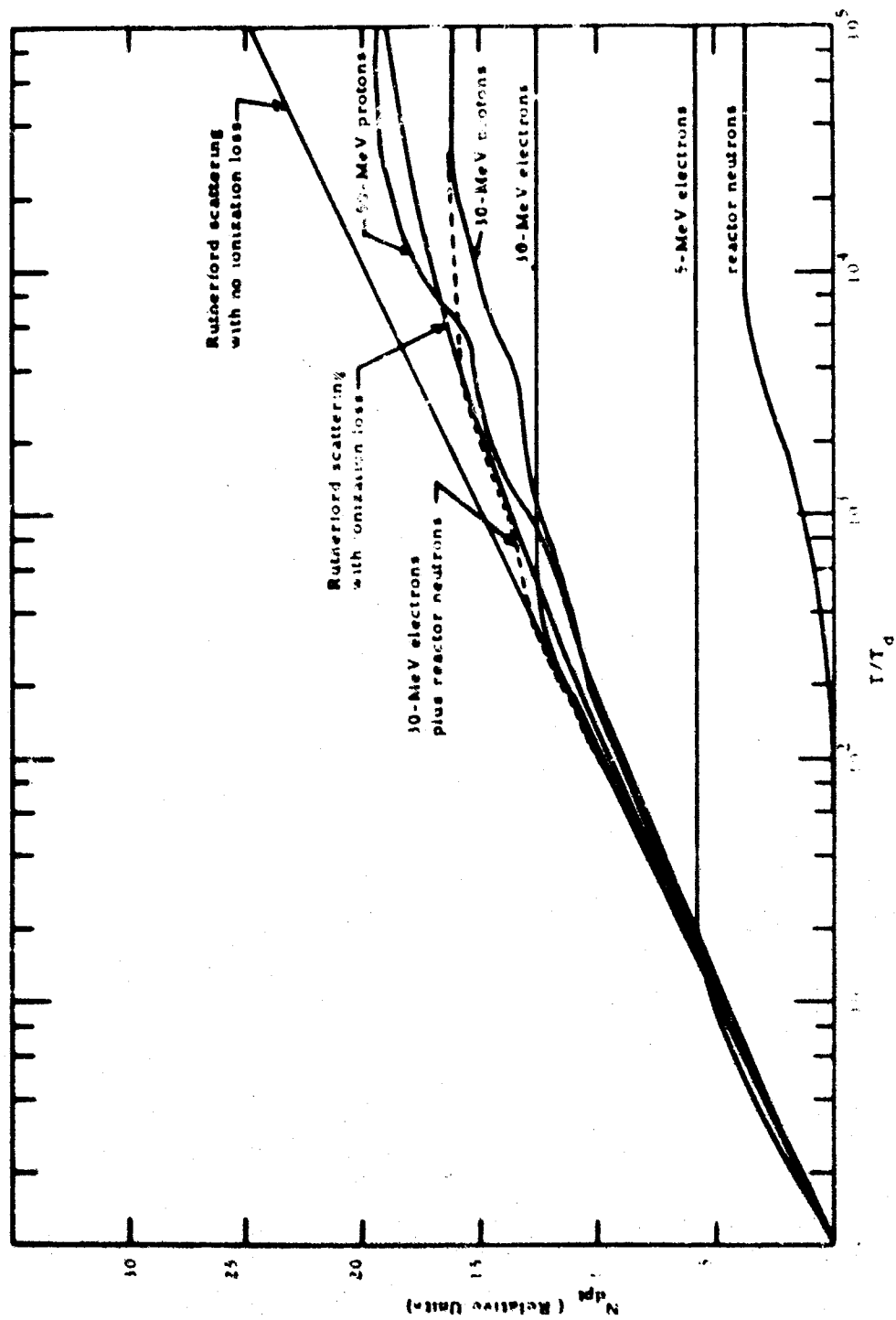
Figure 10. Total number of displaced atoms produced by recoil atoms with energy from T_d to T versus T for germanium

expected from pure Rutherford scattering using both the computed value of f and f = 1 for the case where all of the recoil energy is assumed to be dissipated in displacement type collisions.

2.6. ELECTRON DAMAGE

The electron energies of 5 and 30 MeV considered here are in the relativistic range, so the calculations of McKinley,[14] which are plotted in Fig. 11, were used for the ratio of the scattering cross section to the Rutherford cross section, $d\sigma/d\sigma_R$. Then, for the differential scattering cross section,

$$\frac{d\sigma}{dT} = \frac{d\sigma}{d\sigma_R} \frac{vb^2}{4} \frac{T_m}{r^2}$$

where for the relativistic range for electrons, b is contracted by $\gamma = (1 - \beta^2)^{-1/2}$ in which $\beta = v/c$, v is the electron velocity and c is the velocity of light, and

$$T_m = 2 \frac{E_0(E_0 + 2m_0c^2)}{M_A c^2}$$

in which E_0 is the electron kinetic energy, m_0 is the electron mass, and M_A is the mass of the target atom. The differential energy cross section then reduces to

$$\frac{d\sigma}{dT} = \frac{d\sigma}{d\sigma_R} 2\pi \frac{Z^2 e_0^4}{M_A c^2 T^2}.$$

Analogous to the proton case,

$$N_{de}(T_i) = 0.462 \frac{\pi Z^2 e_0^4}{M_A c^2 T_d} \frac{\overline{d\sigma}}{d\sigma_R}\bigg|_{T_i} \overline{i}_{T_i} \tag{4}$$
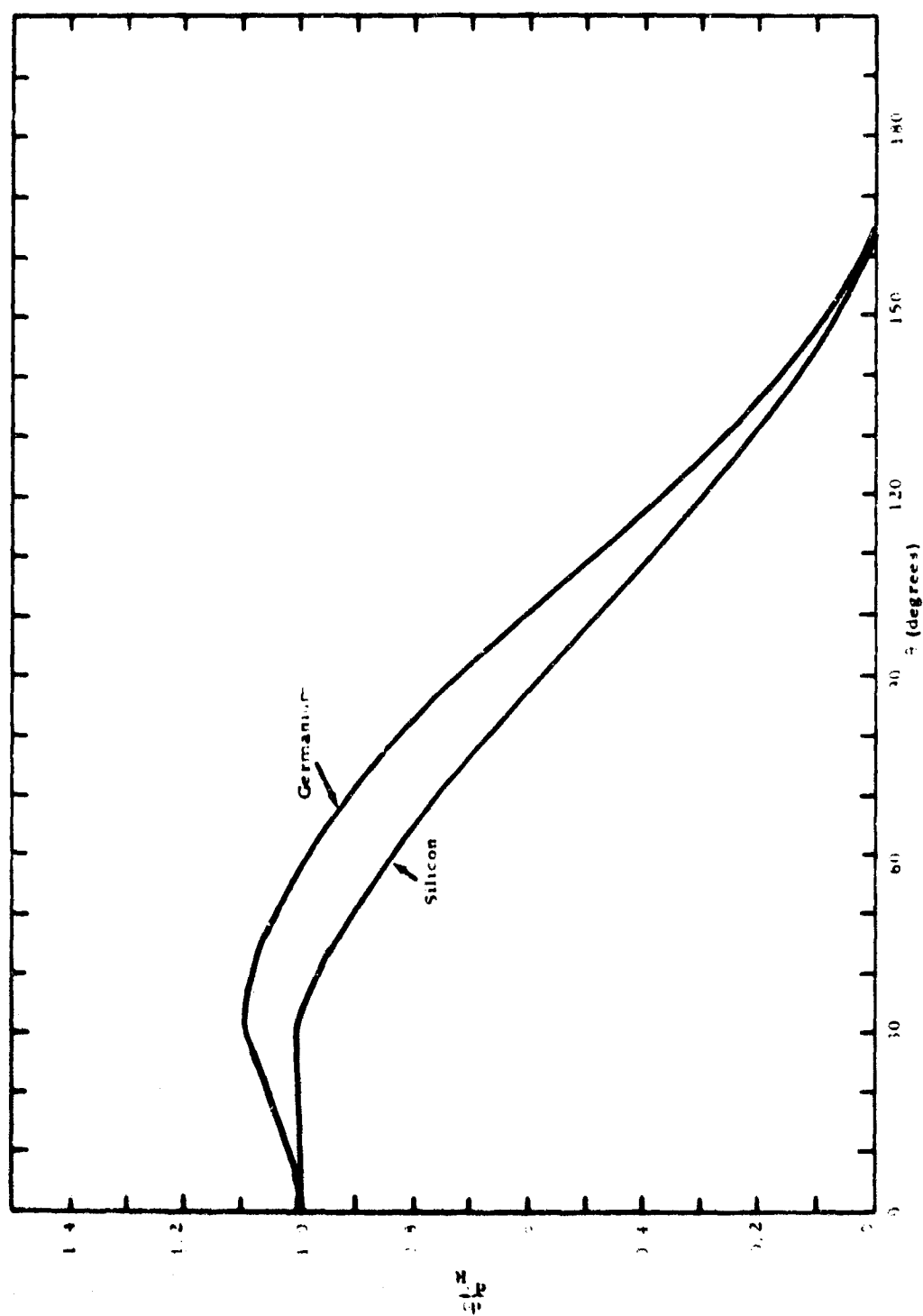
Figure 11. Ratio of scattering cross section to Rutherford cross section vs recoil energy for electrons of energy ≥ 4 MeV

21

and

$$N_{det}(T_i) = 0.462 \frac{\pi Z^2 e_0^4}{M_A c^2 T_d} \sum_{T_d}^{T_i} \frac{\overline{d\sigma}}{d\sigma_R}\bigg|_{T_i} \overline{f}_{T_i} . \tag{5}$$

Equations (4) and (5) are also plotted in Figs. 7 through 10 for 5-
and 30-MeV electrons. These are given in units of $0.462 \pi Z^2 e_0^4/M_A c^2$ for
direct comparison with the primary recoil atom energy spectra of protons.

2.7. NEUTRON DAMAGE

The neutron spectrum used for damage calculations is that calculated
by Larsen[15] for a position in the shielding water 11 in. above the TRIGA
reactor. The logarithmic energy intervals used are the same as those used
for the previous sections. Figure 12 shows the spectrum in terms of neutrons
in each energy interval used. The constancy of the spectrum at lower
energies is a reflection of the 1/E spectrum assumed at energies less than
10 keV.

At neutron energies much above a few hundred keV, the scattering
is markedly anisotropic, so it was necessary to use the angular distributions
of the elastic scattering given in Ref. 16. The resonances particular to
separate elements were smoothed in the calculation by taking rather coarse
energy increments. As was done with protons and for the same reasons,
the measurements on aluminum and copper were used. These angular dis-
tributions were normalized to 1 barn and interpolations were made when
necessary. The normalized angular distributions used for each neutron
energy interval are shown in Figs. 13 and 14 for silicon and germanium,
respectively. These normalized angular distributions were then weighted
by the total cross section from Ref. 17. The results are shown in Fig. 15.

The cross section for producing a recoil atom with an energy ΔT_i
around T_i from a scattered neutron of energy E_n is
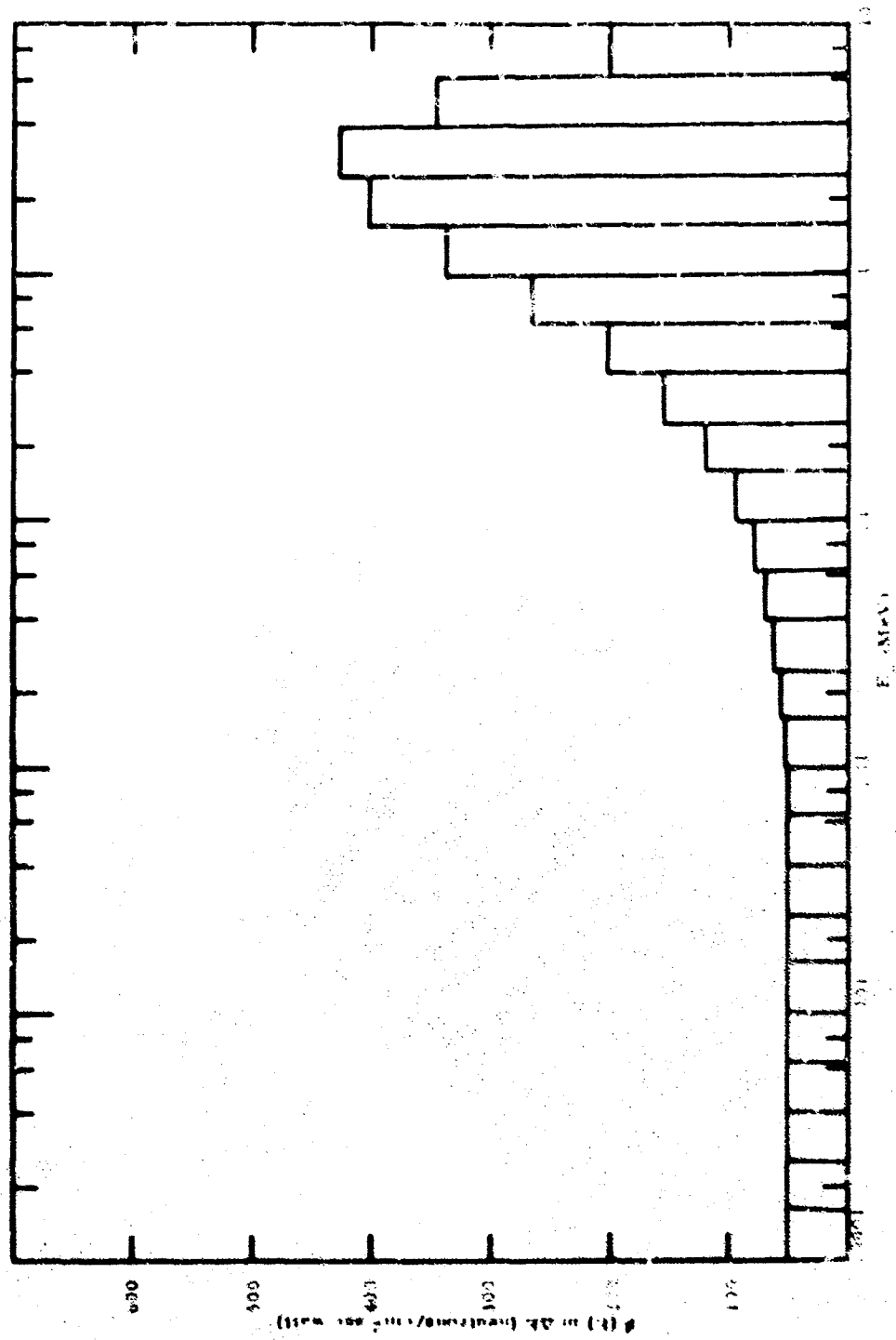
Figure 12. TRIGA neutron spectrum 11 in. above reactor

23
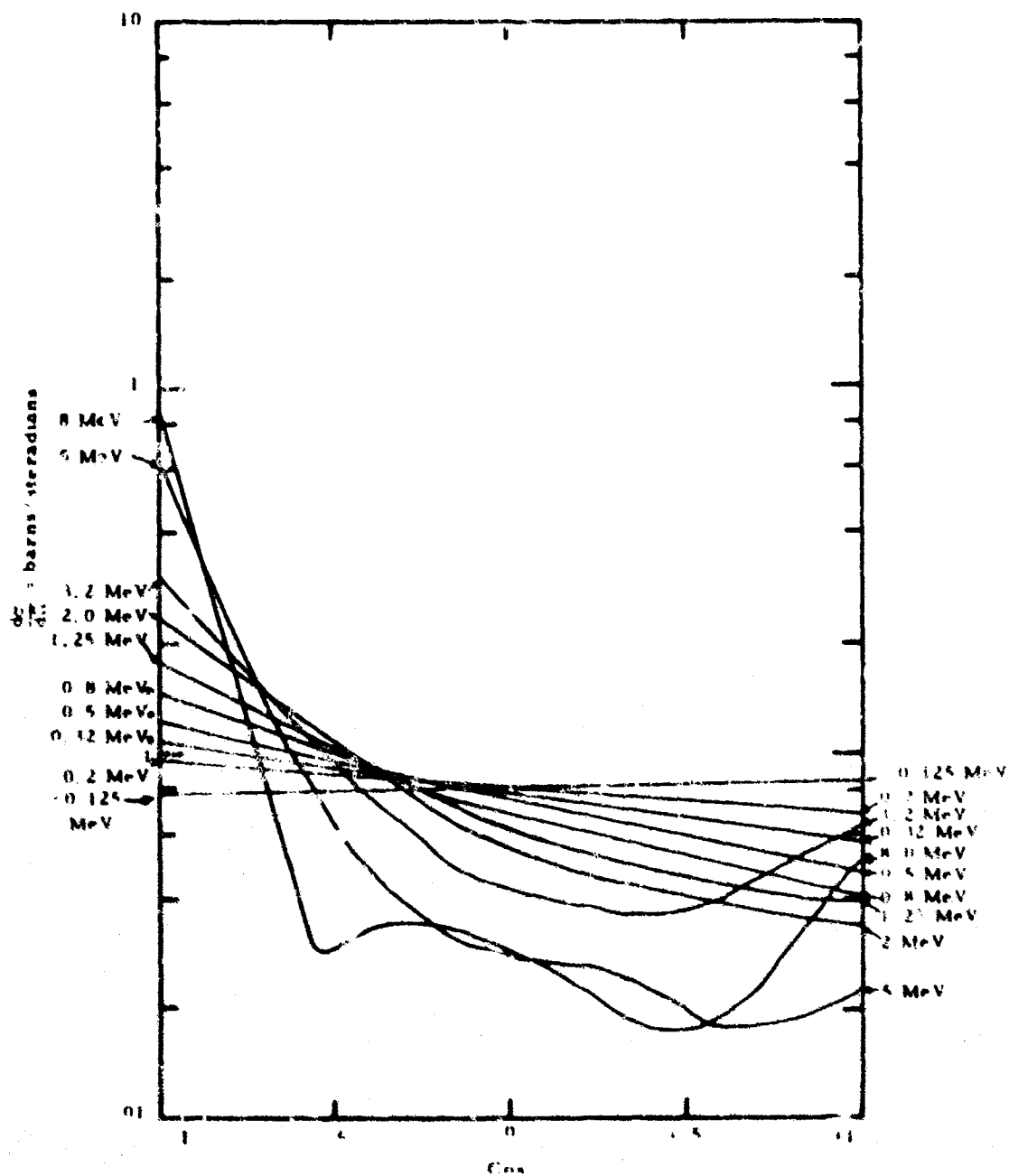
Figure 13. Angular distributions used for neutrons scattered by silicon, normalized to 1 barn, vs the cosine of the scattering angle

24
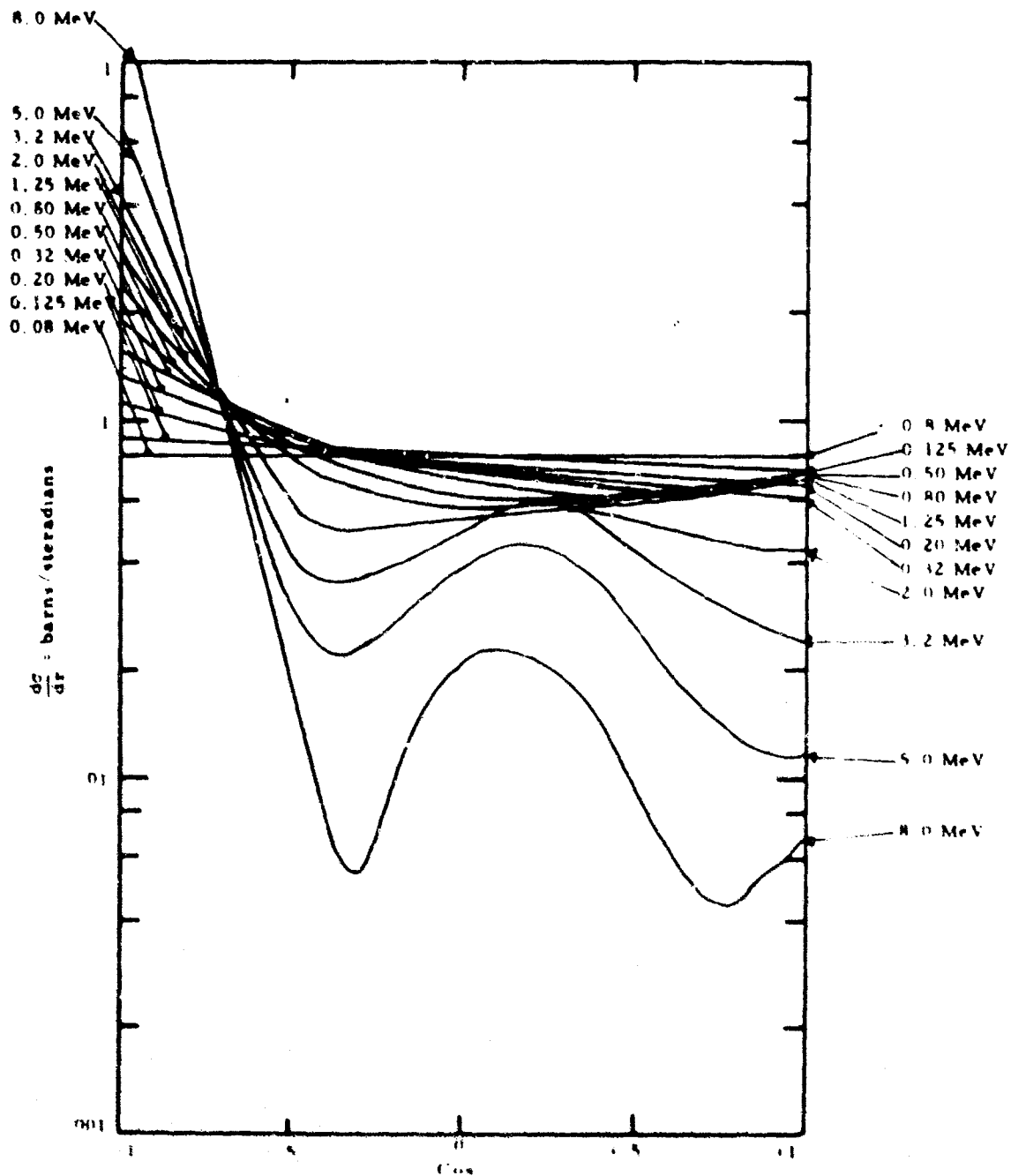
Figure 14. Angular distributions used for neutrons scattered by germanium, normalized to 1 barn, vs the cosine of the scattering angle

25
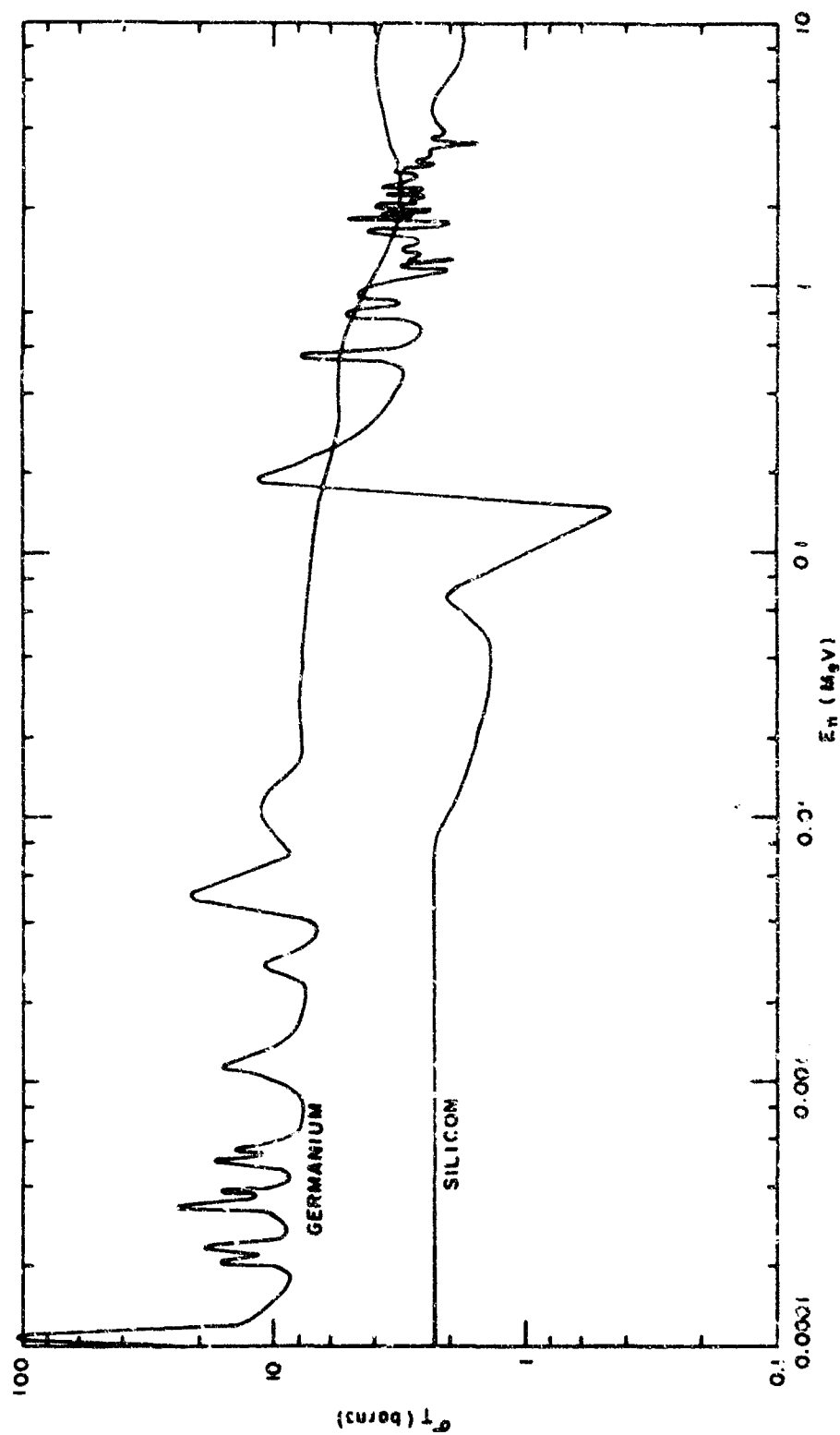
Figure 15. Total neutron elastic scattering cross sections for silicon and germanium

26

$$\Delta T_i \frac{d\sigma}{dT}\bigg|_{E_n, T_i} = \frac{4\pi}{\hat{T}_{E_n}} \frac{d\sigma}{d\Omega}\bigg|_{E_n, T_i} \Delta T_i \frac{barns}{atom} ,$$

where

$$d\sigma/dT\bigg|_{E_n, T_i} \quad \text{and} \quad d\sigma/d\Omega\bigg|_{E_n, T_i}$$

are the differential energy and angular cross sections, respectively, evaluated at E_n and T_i, and $\hat{T}_{E_n}$ is the maximum energy that may be imparted to a recoil atom with a neutron of energy E_n.

The cross section for producing displacements per watt-second of reactor power due to recoils of energy ΔT_i around T_i from scattered neutrons of incident energy ΔE_n around E_n, $N_{dn}(E_n, T_i)$, is just the cross section for producing a recoil atom with an energy ΔT_i around T_i times the number of neutrons incident with energy ΔE_n around E_n per watt-second of reactor power times the number of displacements per recoil atom, i.e.,

$$N_{dn}(E_n, T_i) = \left[\frac{4\pi}{\hat{T}_{E_n}} \frac{d\sigma}{d\Omega}\bigg|_{E_n, T_i} \Delta T_i \right] \left[\phi(E_n)\Delta E_n \right] \left[\bar{f}_{T_i} \frac{T_i}{2T_d} \right] \times 10^{-24} , \quad (6)$$

where $\phi(E_n)\Delta E_n$ is given in Fig. 12 and the factor of 10^{-24} converts the cross sections from barns to square centimeters.

Then the cross section for producing displacements per watt-second of reactor power due to recoils of energy ΔT_i about T_i, $N_{dn}(T_i)$, using $\Delta T_i = 0.465 \, T_i$ for our logarithmic energy intervals and $\hat{T}_{E_n} = (4/A)[1 + (1/A)]^{-2} E/n$, is

$$N_{dn}(T_i) = 0.730 \times 10^{-24} \frac{A}{T_d} \left(1 + \frac{1}{A} \right)^2 \bar{f}_{T_i} \sum_{E_n} \phi(E_n)\Delta E_n \frac{d\sigma}{d\Omega}\bigg|_{E_n, T_i} \frac{T_i^2}{E_n} , \quad (7)$$

where the summation extends over the reactor neutron spectrum from the maximum energy $E_n = 8$ MeV down to $E_n = (A/4)[1 + (1/A)^2]T_i$, the least energetic neutron that can give energy T_i to a recoil.

27

Also, the total cross section for displacements produced by recoil atoms with energy from T_d to T_i, $N_{dnt}(T_i)$, is

$$N_{dnt}(T_i) = 0.730 \times 10^{-24} \frac{A}{T_d} \left(1 + \frac{1}{A}\right)^2 \sum_{T_j=T_d}^{T_j=T_i} \bar{f}_{T_j} T_j^2 \sum_{E_n} \phi(E_n) \Delta E_n \frac{d\sigma}{d\Omega}\bigg|_{E_n,T_j} \frac{1}{E_n} ,$$

(8)

which is analogous with that for protons. Equations (7) and (8) are plotted in Figs. 7 through 10 in units such that the total number of displacements due to neutrons is equal to the difference in the total number of displacements produced by 30-MeV protons and 30-MeV electrons, when the proton and electron displacement production rates are matched at low recoil energies.

2. 8. CONCLUSIONS

A complete discussion of the theoretical results without the experimental comparison is inappropriate here except for a few basic conclusions. From an inspection of Figs. 7 and 9, the general features of the primary recoil atom spectra from electron, proton, and reactor neutron collisions are quite clear. Electrons produce displacements at a nearly constant rate as the primary recoil energy or, equivalently, the displacement cluster size is increased up to nearly the maximum energy recoil. The maximum energy recoil is approximately proportional to the square of the incident electron energy, instead of being linear as with protons, because the relativistic mass of the electron increases with energy. For protons, nuclear elastic scattering produces oscillations in the displacement production cross section. The positions of these oscillations are nearly constant in recoil atom energy as the incident proton energy is increased, with new oscillations being introduced as the incident proton energy and maximum atom recoil energy are increased. The enhancement of the scattering cross section due to nuclear elastic scattering as the incident energy is increased is primarily due to the growth of the first one or two peaks in the scattering

28

cross section. The effect of subsequent peaks is reduced by the function, f, which is the fraction of recoil energy going into displacement-type collisions. From an inspection of Figs. 3 and 4, it can be seen that nuclear elastic scattering is important to quite low incident proton energies, especially in silicon.

When 30-MeV electron irradiations are compared with proton irradiations, the deviation in displacement production occurs only for displacement clusters of ~500 displaced atoms for germanium and ~1000 displaced atoms for silicon. When 5-MeV electrons are considered, the electron simulation is much less likely to be successful since the clusters scale only to 10 and 20 displaced atoms for germanium and silicon, respectively.

Table I summarizes the results of these calculations with a displacement energy T_d equal to 25 eV for silicon and 32 eV for germanium. The second column presents the relative magnitude of the low-energy portion of the Rutherford scattering cross section, i.e., a number by which the fluence of particles should be divided to achieve the same number and spectrum of low-energy recoils. The third column presents the recoil energy, in units of T_d, above which the total displacement energy deviates by more than 20 percent from the Rutherford value for large maximum energy transfer, but with corrections for ionization energy loss. This quantity is a measure of the range of validity of the low-energy recoil spectrum simulation. The last column presents the effective cross section for producing displaced atoms, irrespective of the size of the cluster with which the atoms are associated. Again, this number should be used only for relative magnitudes since most of the displaced atoms undergo thermally activated rearrangement at room temperature.

It is apparent from the foregoing calculations that the best simulator for proton irradiations to meet the two conditions discussed in Section 2.1 is a combination of high-energy electron and neutron irradiation. Specifically, the following correlations are indicated:

29

Table I

THEORETICAL PREDICTIONS OF THE STRUCTURE OF THE PRIMARY RECOIL ENERGY
SPECTRA FROM DIFFERENT PARTICLE IRRADIATIONS

Incident Radiation	Silicon			Germanium		
	Relative Number of Low-Energy Recoils	Rutherford Scaling Limit (T/T_d)	Displacement Cross Section (barns)	Relative Number of Low-Energy Recoils	Rutherford Scaling Limit (T/T_d)	Displacement Cross Section (barns)
TRIGA neutrons (not >10 keV)	0	- - -	2510	0	- - -	1610
50-MeV protons	8.4	130	2060	13.2	120	2580
30-MeV protons	13.9	110	3040	22	120	3610
30-MeV electrons	0.90	720	114	1.42	350	180
5-MeV electrons	0.90	25	66	1.42	12	83
2.3-MeV electrons	0.90	5	46	1.42	3	49
1.5-MeV electrons	0.90	3	35	1.42	1	33

30

In silicon:

One 30-MeV proton/cm^2 = 15.5 14-MeV electron/cm^2 +
0.62 TRIGA neutrons/cm^2

One 50-MeV proton/cm^2 = 9.3 14-MeV electron/cm^2 +
0.47 TRIGA neutrons/cm^2

In germanium:

One 30-MeV proton/cm^2 = 15.5 20-MeV electrons/cm^2 +
0.73 TRIGA neutrons/cm^2

One 50-MeV proton/cm^2 = 9.3 20-MeV electrons/cm^2 +
0.70 TRIGA neutrons/cm^2

where this electron energy is chosen to simulate the first dip in the proton nuclear elastic scattering cross section.

In lieu of irradiations with electrons and neutrons, it may be hoped that less accurate but satisfactory simulation is possible with electrons alone, using a scaling factor based on total number of displacements irrespective of primary recoil energy. In essence, this scaling replaces some of the higher-energy proton-induced recoils by low-energy recoils. The electron simulation will then overestimate or underestimate the damage, depending on whether the physical property measured, taking into account thermal motion, is more or less sensitive to the same number of displaced atoms being distributed in smaller recoil clusters. The damage ratios on this basis are as follows:

	Silicon	Germanium
$\dfrac{\text{30-MeV protons}}{\text{30-MeV electrons}}$:	27	20
$\dfrac{\text{50-MeV protons}}{\text{30-MeV electrons}}$:	18	14
$\dfrac{\text{5-MeV electrons}}{\text{30-MeV electrons}}$:	0.58	0.46
$\dfrac{\text{2.3-MeV electrons}}{\text{30-MeV electrons}}$:	0.42	0.29
$\dfrac{\text{1.5-MeV electrons}}{\text{30-MeV electrons}}$:	0.24	0.11

31

It should also be noted that the difference in the contribution of higher-energy primary recoils due to nuclear elastic scattering between 30- and 50-MeV protons is found to be less than the enhancement of higher-energy recoils by nuclear elastic scattering over Rutherford scattering at 30 MeV. It was found that for silicon, the contribution from nuclear elastic scattering with 30-MeV protons is twice the increase in nuclear elastic scattering when going from 30- to 50-MeV protons. It is somewhat different for germanium in that for 30-MeV protons, nuclear elastic scattering decreases the damage calculated, assuming pure Rutherford scattering, by approximately the same amount that changing from 30- to 50-MeV increases it. The 50-MeV irradiations thus only serve to check results obtained at 30 MeV, and both energies will be affected significantly by nuclear elastic scattering.

SECTION III

EXPERIMENTAL PROCEDURES

3.1 SAMPLE PREPARATION

3.1.1 Sample Cutting and Identification

The irradiation samples were cut from the semiconductor boule in the manner shown in Fig. 16. First, 2-mm-thick slices were cut from the boule; they were then remounted and cut into bars 1 mm thick by 20 mm long. Of the six slices taken, alternate slices (H1, H2, and H3) were used for the Hall coefficient studies and the other slices (τ1, τ2, and τ3) were used for carrier lifetime studies. Each sample was identified, as shown, as to its origin and eventual use. A seventh slice was taken after the τ3 slice and cut into bars for the unir adiated samples required. The A_3 and A_4 pieces outside the A_2 samples were cut 1/2 and 1/4 mm thick to provide samples for the 2.3 and 1.5-Mev electron irradiations, respectively.

The sample bars were lapped successively with 400-grit, 600-grit, 2/0, and 4/0 emery papers and then they were etched. The germanium samples were etched in Super-oxal etching solution (1 part hydrofluoric acid, 1 part hydrogen peroxide, and 4 parts water), whereas the silicon samples were etched in a "white" etching solution (equal parts of glacial acetic, nitric, and hydrofluoric acids). After the samples were etched, they were rinsed in distilled water and electronic-grade alcohol. The preparation of the sample for irradiation then varied according to the type of sample.

3.1.2 Preparation of n-Type Silicon

Each n-type silicon sample was placed in a quartz jig for the gold-bonding operation. The jig held small dots of 0.5 percent antimony-doped

33

Scribe line along length of boule

Semiconductor Boule

1.5 MeV e⁻
2.5 MeV e⁻
5 MeV e⁻
30 MeV e⁻
30 MeV p⁺
50 MeV p⁺

H τ1 H2 τ2 H3 τ3

H = Hall Samples

τ = Lifetime Samples

A₁
A₃
A₂
A
B
B₂

Material	Supplier Code	Boule Length in mm	Dopant	Resis-tivity	Type	Pulled	Sample distance from boule bottom in mm	30 MeV Electron Sample	Middle Hall Sample
S1	Mo	73	- P	- 10	N	2	- 71	A	- H2

Figure 1b. Sample cutting and identification

34
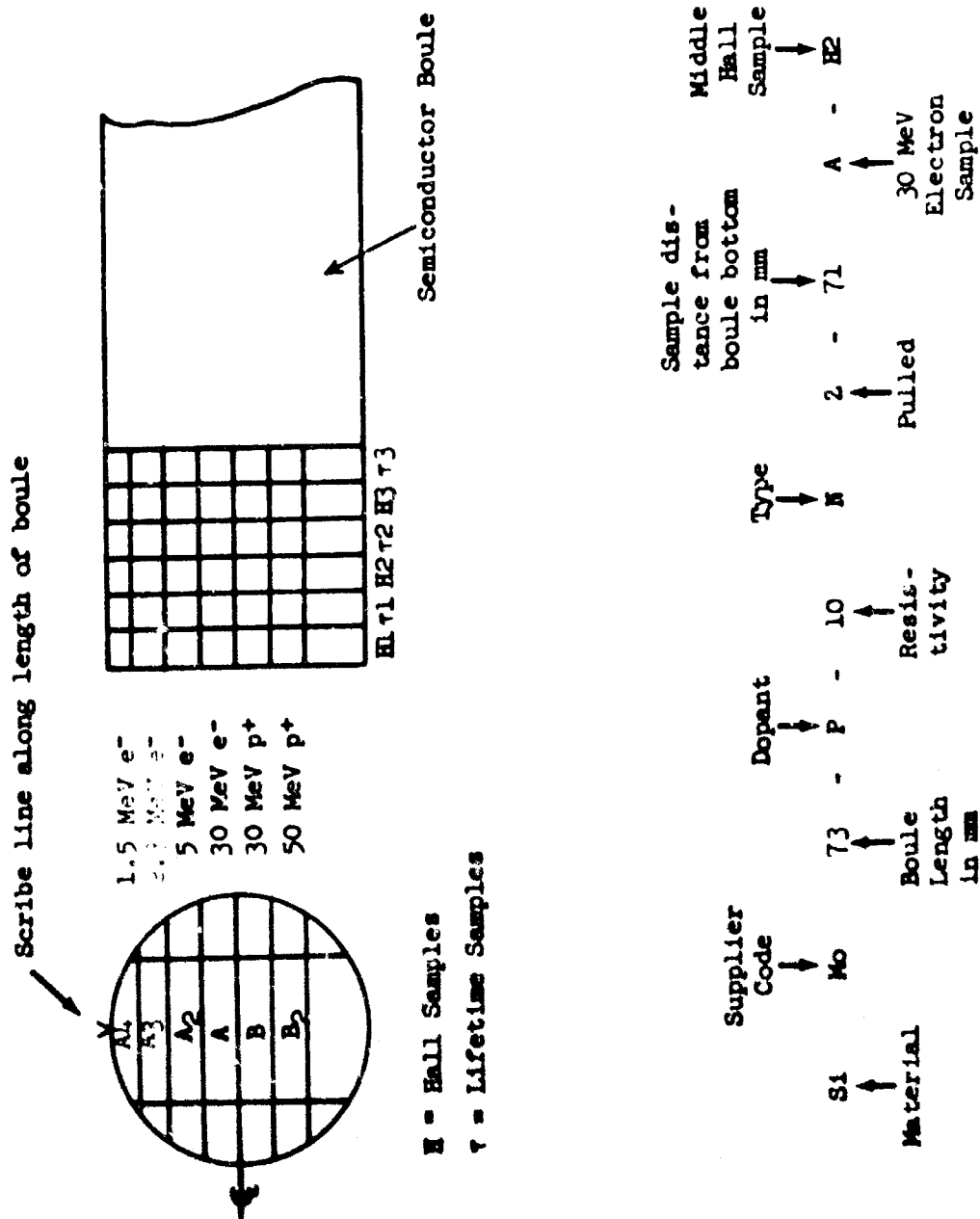
gold against the sample at the voltage and Hall lead positions. The jig was spring loaded to allow for contractions due to the melting of the gold dots during the bonding. The jig and sample were then placed in an oven heated to 450°C for about 5 min in a flow of forming gas and then they were cooled slowly. After cooling, the sample was removed from the jig and the ends for the current leads were first roughened with 600-grit emery paper and then nickel plated. The electroplating solution consisted of 105 parts by weight of nickel ammonium sulfate, 15 parts of ammonium chloride, and 15 parts boric acid. The sample was then washed in alcohol and acetone and the plated ends were tinned with indium solder.

A 1-mil copper wire was soldered to each gold button to provide the sample lead. A copper-constantan thermocouple was soldered to 1 gold button and used as a Hall lead on the Hall coefficient samples. The thermocouple was attached at a current lead for the carrier lifetime samples. Soldering to the gold buttons was accomplished by first tinning the copper wire, leaving a small ball of solder on the end. The solder ball was then heated in contact with the gold button with a small jet of hot helium gas. Usually a little Ruby fluid flux was needed to fuse the solder to the gold. Current leads were then soldered to the ends of the sample, which was then washed in alcohol to complete the preparation of the sample.

3.1.3 Preparation of p-Type Silicon

The procedure for preparing the p-type silicon samples differed from that used for n-type silicon in that boron-doped gold dots were used and the current ends were plated with a rhodium plating solution obtained from Englehard Industries, Inc. Alternatively, point contacts were sometimes used for Hall and voltage probes. These were phosphor-bronze wires with the ends pointed and coated with aluminum that were spring loaded against the sample. Contact was made by fusing the wire to the sample by passing the current from a spark coil through the contact.

35

3.1.4 Preparation of n-Type Germanium

For n-type germanium the Hall and voltage leads were made by first placing four small pieces of 60/40 soft solder on the sample. The solder pieces were held in place by the surface tension of the Ruby fluid flux used to facilitate soldering. The sample was then placed in an oven which consisted of a glass tube wound with a heater. A flow of an inert gas was maintained through the glass tube, and the sample was heated to the melting point of the solder to bond the solder dots to the sample. The ends of the sample were tinned directly with indium solder for the current leads. Leads were attached in the same manner as those for n-type silicon.

3.1.5 Preparation of p-Type Germanium

The preparation of p-type germanium differed from n-type only in that indium solder was used for all contacts.

3.2 HALL EFFECT

Samples irradiated for measurement of carrier removal rate were mounted as shown in Fig. 17 with phosphor-bronze spring clips holding the samples to an aluminum block. The samples were electrically insulated from the block and clips with Mylar adhesive tape. The block was then placed in a water-cooled chamber, as shown in Fig. 18, so that the H1 sample was nearest the lid and the H2 sample was in the middle. The electrical leads of the H2 sample were the only ones brought out of the box. The Hall coefficient of the H2 sample only was monitored during irradiation; the other two samples were measured in the laboratory before and after irradiation as a check.

A thermally conductive path from the aluminum block to the sample chamber was formed by using tin-foil shims between the block and the bottom and lid of the sample chamber. The chamber was also filled with helium gas during irradiation for more efficient heat transfer.

36

Phosphor-Bronze
Spring Clips

Mounting Block

Semiconductor Samples
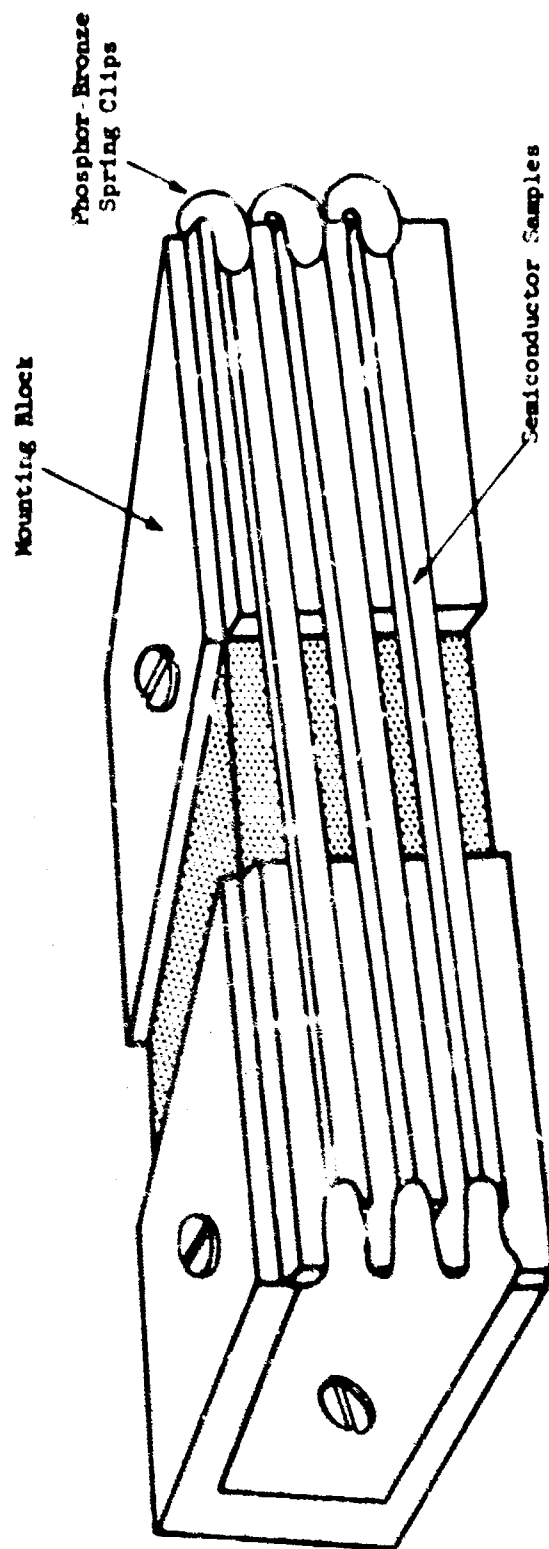
Figure 17. Sample mounting

EVACUATING TUBE

010" ALUMINUM ACCELERATOR WINDOW

COOLANT EXIT TUBE

COOLANT CHAMBER

FALSE BOTTOM

ELECTRICAL LEADS

COOLANT INLET TUBE
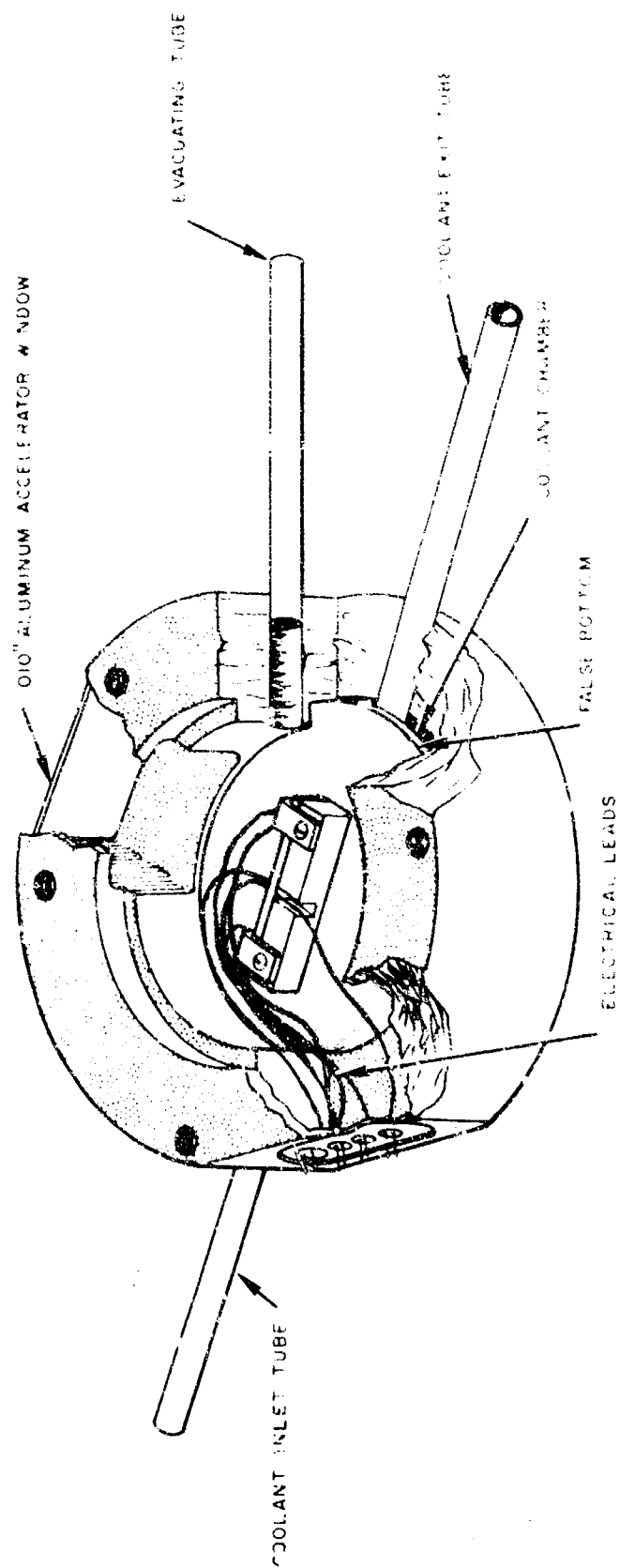
Figure 18. Irradiation chamber for samples

38

Hall coefficients were measured in a field of 4 kgauss with a current of about 2 ma passing through the sample. The sample Hall probes were connected to a microvolt ammeter through a voltage bucking box to cancel out any potential difference at zero magnetic field due to misalignment of the probes. The meter drove a chart recorder and thus a record was made of the Hall voltage at opposite polarities of the magnetic field. The difference in the two Hall voltages was used to calculate the carrier density in order to cancel out any contact effects. The current passing through the sample was measured by monitoring the voltage drop across a 1-kΩ series resistor.

Hall coefficients were measured at the irradiation site before the samples were irradiated and the irradiation was interrupted at appropriate intervals for further measurements until the Hall voltage had changed by 25 percent, at which time the irradiation was terminated. Irradiated samples were then taken to the laboratory and there the Hall coefficient was measured at room temperature after successive 5-min anneals at 325°, 345°, 367°, 388°, and 400° K.

A temperature record of the H2 samples was made during the irradiations and the beam intensity was controlled to limit the temperature rise to a few degrees Kelvin.

3.3 CARRIER LIFETIME

Carrier lifetime samples were mounted in triple mounts in much the same manner as the Hall samples were, but because the rate of lifetime damage was generally much higher, sample heating was much less of a problem and thus plug-in mounts were developed, as shown in Figs 19 and 20. The miniature 9-pin connectors permitted quick sample changing without the delicate operation of manipulating the sample leads themselves. As with the Hall measurements, only one of three lifetime samples was monitored during the irradiation; the other two served as a check and were measured in the laboratory before and after irradiation.

Sample Leads

Light Window

Cooling Chamber Tube

Sample Chamber Gas
Filling Tube

Cooling Chamber Tube

Beam Window
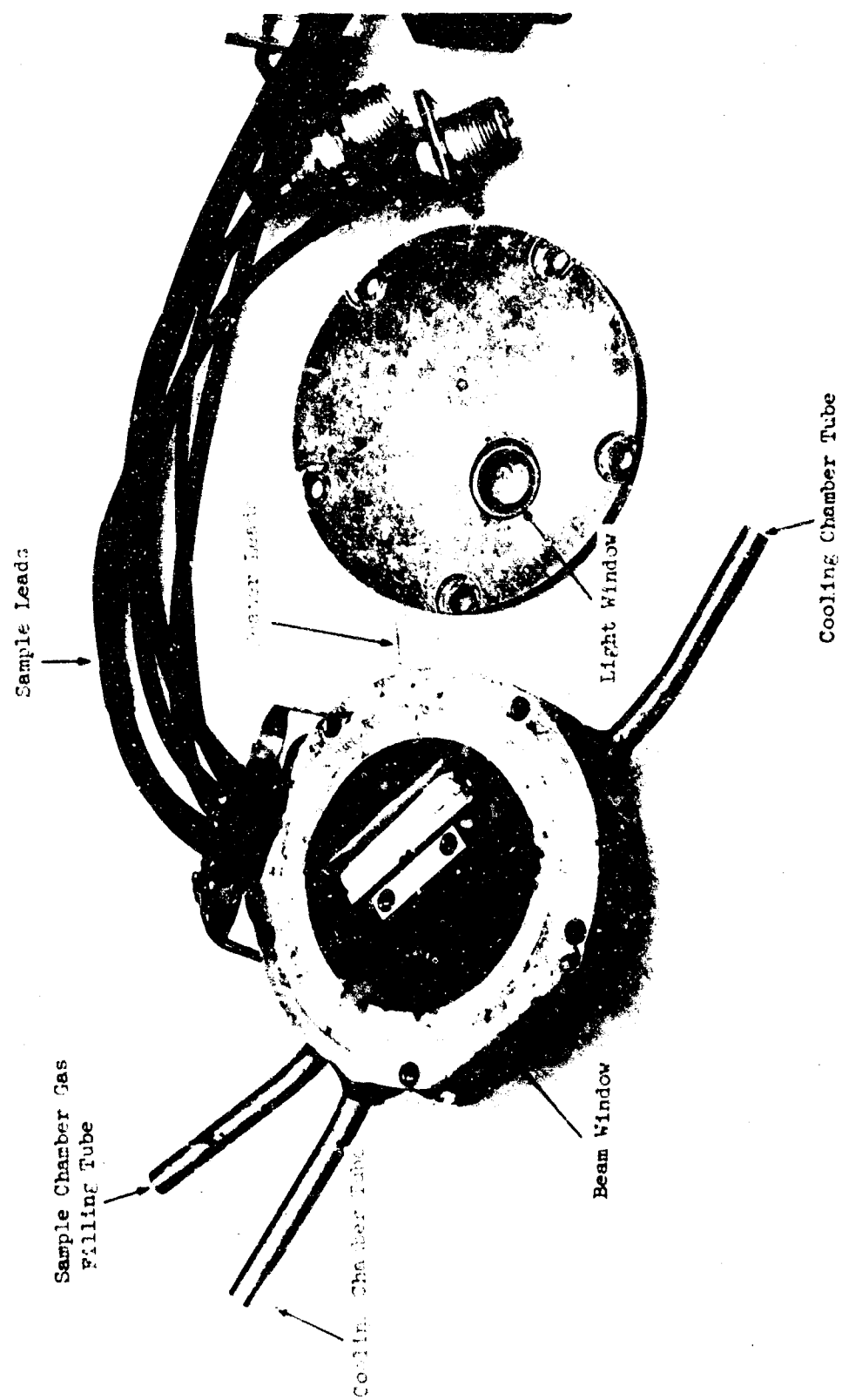
Figure 19. Irradiation sample chamber for lifetime measurements

40
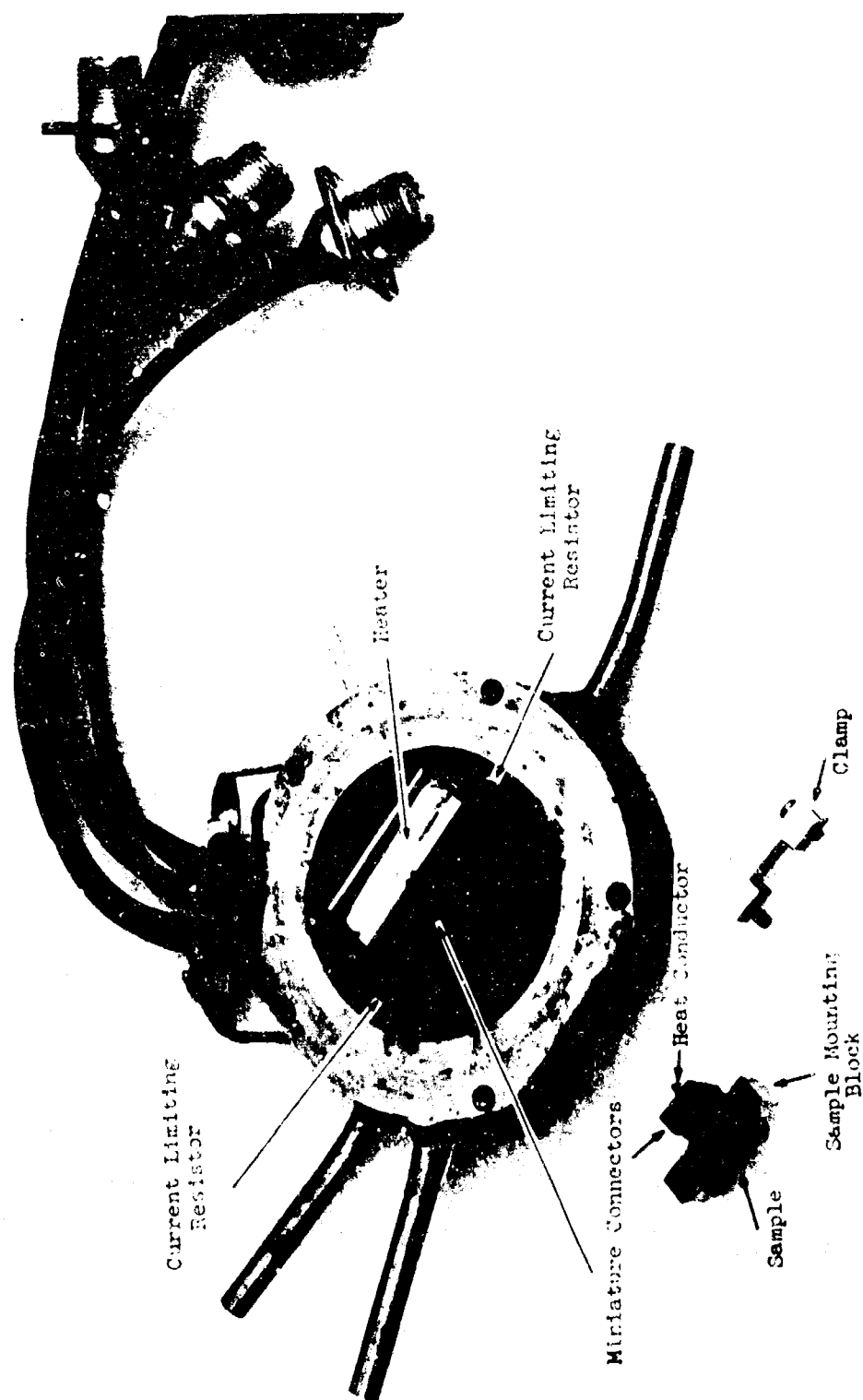
Figure 20. Sample chamber with sample mount unplugged

Current Limiting Resistor

Heater

Current Limiting Resistor

Clamp

Heat Conductor

Sample Mounting Block

Miniature Connectors

Sample

The carrier lifetime was measured by observing the transient conductivity of the sample in a 4-point measurement with carriers injected by a light pulse from a General Radio Strobotac, the General Atomic linear accelerator, or the General Atomic flash X ray. Figure 21 shows the shape of the light pulse at two different repetition rates near the end of the instrument's range. The high-rate pulse was used for the measurements because of the shorter decay time, even though the peak light output is much less. Thus it was necessary to place the light source very close to the sample.

Provision was made for measuring the transient current through the sample, but this was found to be unnecessary because of the high impedance source used. The transient voltage was measured with a dc current of about 2 mA in the sample. Contact effects were minimized by using the difference between the voltage signals taken with opposite polarity currents. Pictures were taken of the transient voltage signal on an oscilloscope camera with the instrumentation presented in block diagram in Fig. 22. The gain of the preamplifier system, consisting of Tektronix Type G plug-ins in a 127 power supply, was remotely controlled by means of Ledex stepping motors on the gain switches of the Type G preamplifiers. The cable drivers are capable of driving the 93-ohm cables connecting the irradiation and control rooms with 1-V peak-to-peak signals. The over-all sensitivity of the system is 0. 5 mV/cm.

Transient voltage signals thus taken were assumed to be inversely proportional to the conductivity (constant-current assumption). The signals plus the dc voltage measured across the sample with no carrier injection were read into a computer program which calculated the carrier lifetime as a function of injection levels. From these data, the lifetime degradation as a function of radiation flux was determined. During electron irradiations, the lifetime measured with the Strobotac was checked against the lifetime measured when a short (0. 1-μsec) pulse of relativistic electrons was used to inject carriers. These measurements were made to calibrate
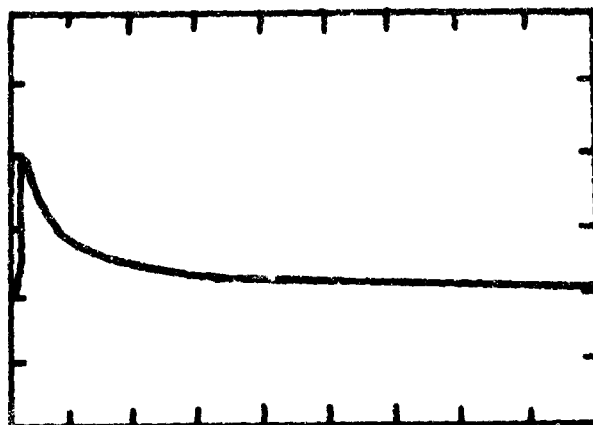
Repetition rate   700 ppm

Sweep   5 μsec/cm
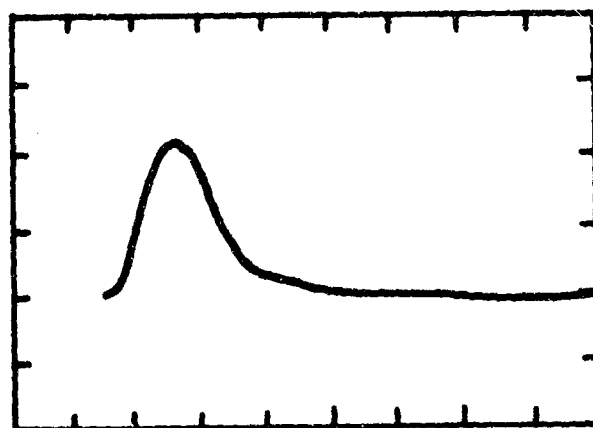
Repetition rate   25,000 ppm

Sweep   0.5 μsec/cm

Figure 21.   Light pulse from General Radio Strobotac
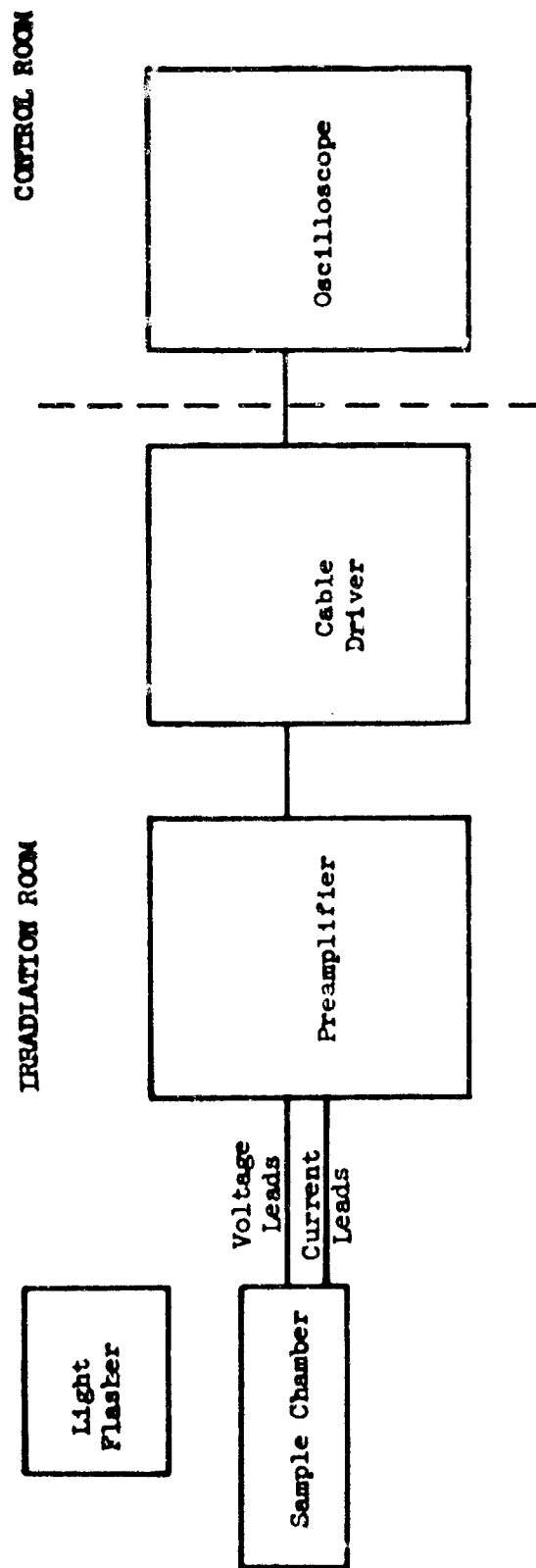
Figure 22. Lifetime instrumentation diagram

the Strobotac for use in off-site irradiations where no other carrier-injection source was available. Because of the length of tail on the Strobotac light pulse and the uneven carrier injection in the sample, measurements with the Strobotac were limited to lifetimes in excess of a microsecond, with the calibration being required when the lifetime was below about 10 μsec.

After irradiation, the samples were put through the same annealing schedule as the Hall samples, with the lifetime being measured with the flash X-ray facility.

3.4 DOSIMETRY

3.4.1 Beam Calibration

Calibration of the irradiation beam was accomplished by use of a thin calorimeter consisting of a small copper block suspended in a constant-temperature environment. Figure 23 shows a cross section of this calorimeter with the copper block suspended in an evacuated water-cooled chamber by fine copper-constantan thermocouple wires. The entrance and exit windows are 1-mil Mylar affixed to the chamber with epoxy.

The sensitivity of the calorimeter for a pulse of radiation delivered in a time short compared to the thermal relaxation time of the calorimeter block can be calculated in terms of the energy deposition. For the case where the copper block is initially at room temperature, the dose, D (Cu), in rads (Cu) is related to the thermocouple voltage increment, ΔV, by

$$D (Cu) = 0.975 \times 10^9 \, \Delta V .$$

Using as the minimum detectable signal a voltage change of 1 μV/sec or a dose rate of 0.975×10^3 rads (Cu)/sec, the minimum average current density and particle flux for the irradiations considered were calculated; the results are presented in Table II. All fluxes encountered at the irradiation facilities were at least five times greater than the minimum detectable.

45

TO REFERENCE JUNCTION

LID

O-RING SEAL FOR LID

HOLLOW KOVAR SEALS

THERMOCOUPLE WIRES

WATER

MYLAR WINDOW

ABSORBER BLOCK

WATER-COOLED WALL

VACUUM
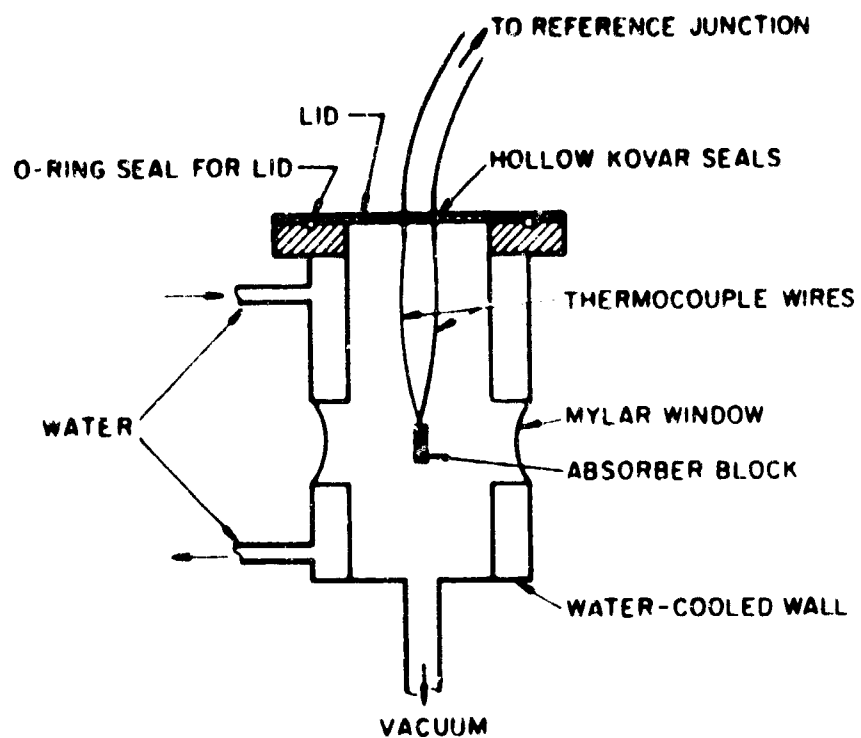
Figure 23. Cross section of thin calorimeter

Table II

AVERAGE CURRENT DENSITY AND PARTICLE FLUX
FOR A 1-μV/SEC CALORIMETER SIGNAL

Incident Radiation	Average Current Density (A/cm^2)	Particle Flux (particles/cm^2 sec)
50-MeV protons	1.23×10^{-9}	7.69×10^9
30-MeV protons	8.34×10^{-10}	5.20×10^9
30-MeV electrons	7.33×10^{-9}	4.58×10^{10}
5-MeV electrons	7.75×10^{-9}	4.84×10^{10}
2.3-MeV electrons	8.06×10^{-9}	5.04×10^{10}
1.5-MeV electrons	8.14×10^{-9}	5.08×10^{10}

3. 4. 2 Beam Monitoring

For continuous monitoring of the beam during irradiation, a secondary-emission monitor was used for both the electron and proton irradiations. It consisted of a 0.008-in. titanium foil in an evacuated chamber with 0.001-in. titanium windows. The monitor was placed between the beam collimator and the sample. The average replacement current to the foil was related to the calorimeter signal when the calorimeter was placed in the sample position in calibration runs before and after each day's irradiations. During the irradiations, the replacement current was monitored on a chart recorder and this record was used, together with the calorimeter calibration, to calculate the incident particle flux.

3. 5 EXPERIMENTAL FACILITIES

The 5-MeV and 30-MeV electron irradiations were performed at the General Atomic Linac, which is an L-band traveling-wave electron accelerator. It can produce pulses of electrons of 3 to 45 MeV, pulse widths varying between 0.01 and 4.5 μsec, repetition rates as high as 720 pps, and beam currents up to 1 A.

The low-energy electron irradiations (1.5 and 2.3 MeV) were performed at the Dynamitron accelerator located at the Convair Division of General Dynamics Corporation in San Diego. It is a cascade-rectifier type of accelerator capable of currents up to 1 mA dc.

The proton linear accelerator at the University of Southern California was used for the initial 31.5-MeV proton irradiations. This accelerator runs at a frequency of 300 Mc, has pulse widths of 450 μsec, and pulse repetition rates of 15 to 20 pps.

The final proton experiments were run at the Oak Ridge National Laboratory, where the synchronous cyclotron was used. This is a dc machine capable of currents in the milliampere range; the energies used were 35 and 56 MeV.

48

Lifetime annealing experiments were performed at the General Atomic flash X-ray facility, which produces 120-μsec pulses of 600-keV X rays with a total dose of about 1 r per pulse.

SECTION IV

EXPERIMENTAL RESULTS

The experimental accuracy attributed to both the Hall coefficient
and the carrier lifetime sample irradiations is about 20 percent, including
both the measurements of the parameters in question and the determination
of the amount of irradiation the samples have received.

4.1 HALL SAMPLE IRRADIATIONS

Considering the Hall effect data first, the typical irradiation
response of 10-ohm-cm phosphorus- and boron-doped materials, both
pulled and floating zone, is shown in Figs. 24, 25, 26, and 27 for a 30-MeV
electron irradiation and a 30-MeV proton irradiation and a 30-MeV proton
irradiation, respectively. The response for corresponding 0.5-ohm-cm
material is shown in Figs. 28, 29, 30, and 31. Similar data for germanium
are shown in Figs. 32 and 33, respectively, for 10-ohm-cm arsenic- and
gallium-doped material during a 30-MeV proton irradiation. The data are
summarized in Table III for the 1.5-, 2.3-, 5-, and 30-MeV electron
irradiation and for the 30- and 50-MeV proton irradiations.

The conductivities measured prior to irradiation are subject to
inaccuracies owing to surface and contact effects. The most meaningful
parameter for sample identification is then, in view of the radiation response
measurements performed, the initial carrier concentration. This is taken
as zero irradiation intercept of the carrier removal curves. his procedure
will give an indication of the initial bulk carrier concentration with the
effects of contacts and surfaces negated to the same degree as they are in
the removal rates. Conductivities may be calculated, if desired, using
known values for the mobility in silicon and germanium. These initial
carrier concentrations are also given in Table III.

50

Figure 24. Carrier removal in 10-ohm-cm n-type silicon irradiated with 30-MeV electrons.

Figure 25. Carrier removal in 10-ohm-cm p-type silicon irradiated with 30-MeV electrons

Figure 26. Carrier removal in 10-ohm-cm n-type silicon irradiated with 30-MeV protons
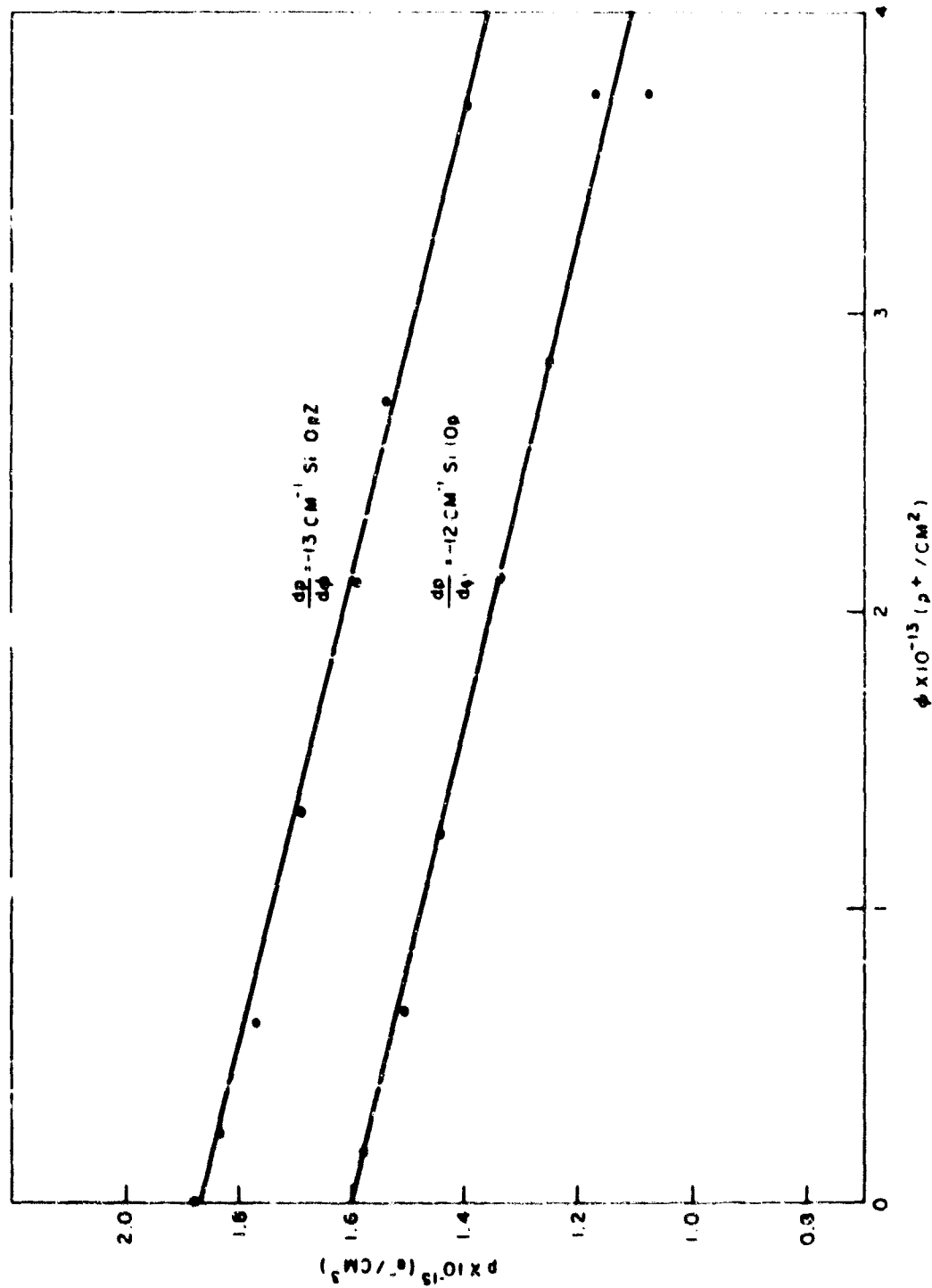
Figure 27. Carrier removal in 10-ohm-cm p-type silicon irradiated with 50-MeV protons

54
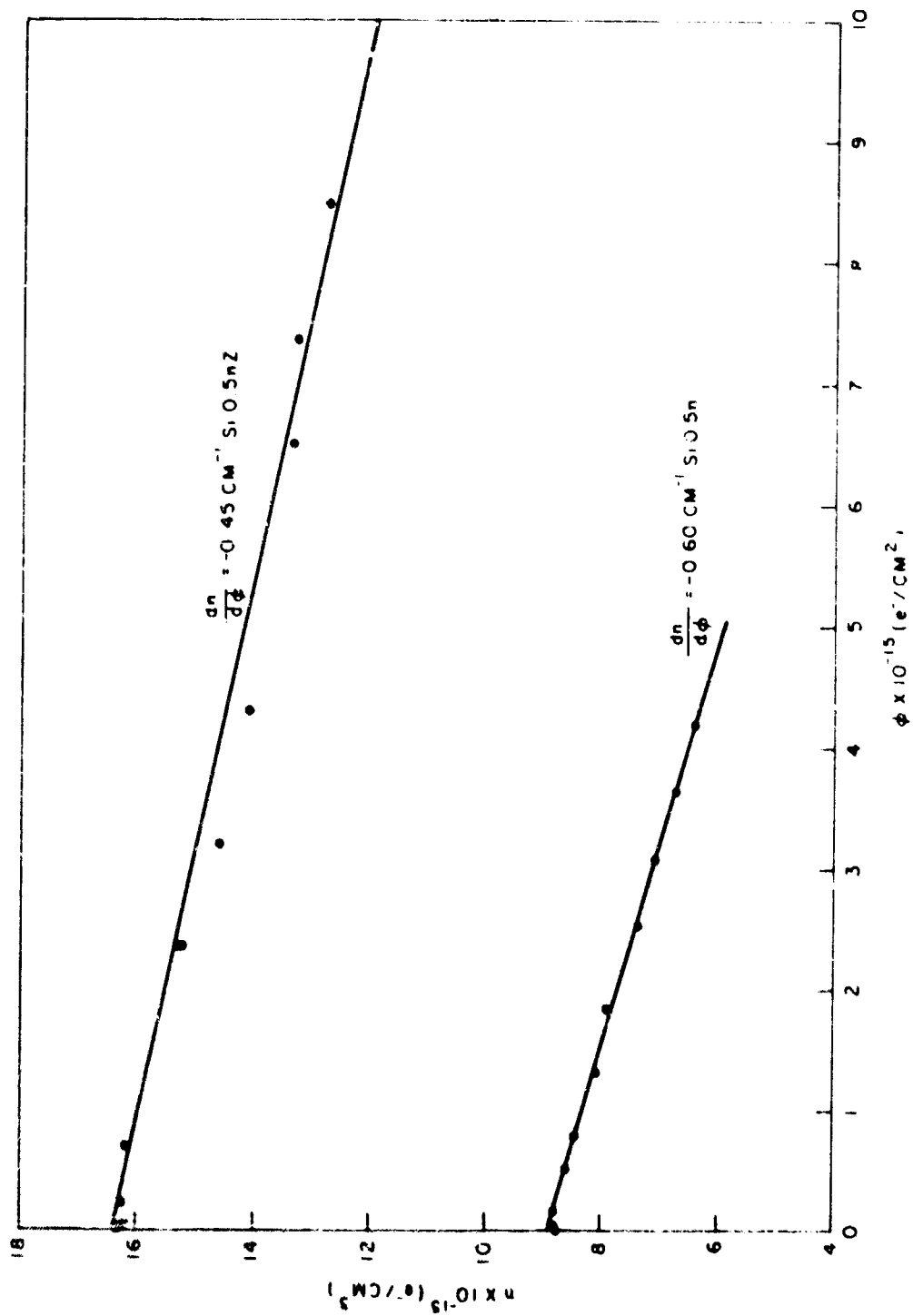
Figure 28. Carrier removal in 0.5-ohm-cm n-type silicon irradiated with 30-MeV electrons

55
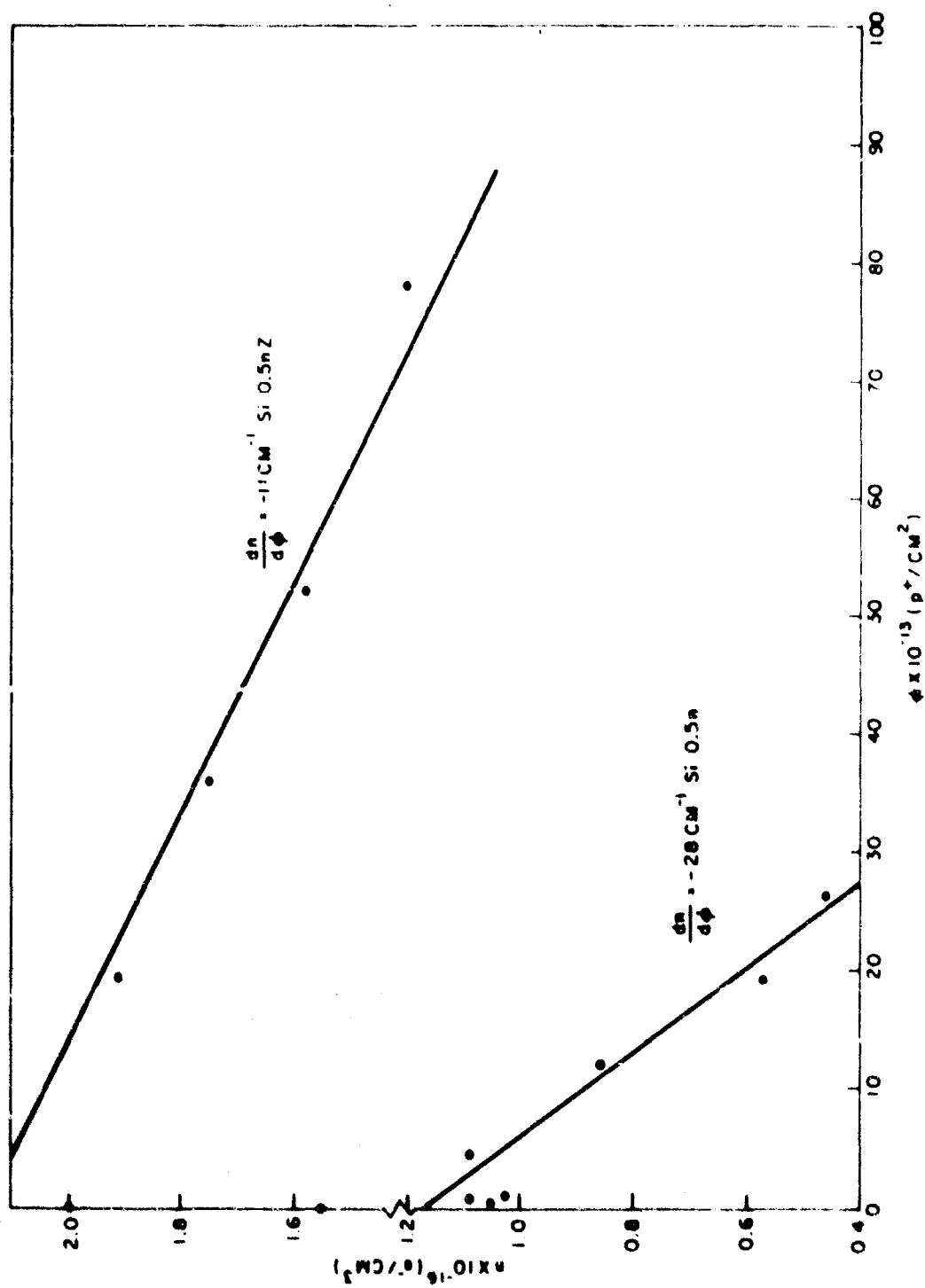
Figure 29   Carrier removal in 0.5-ohm-cm n-type silicon irradiated with 30-MeV protons
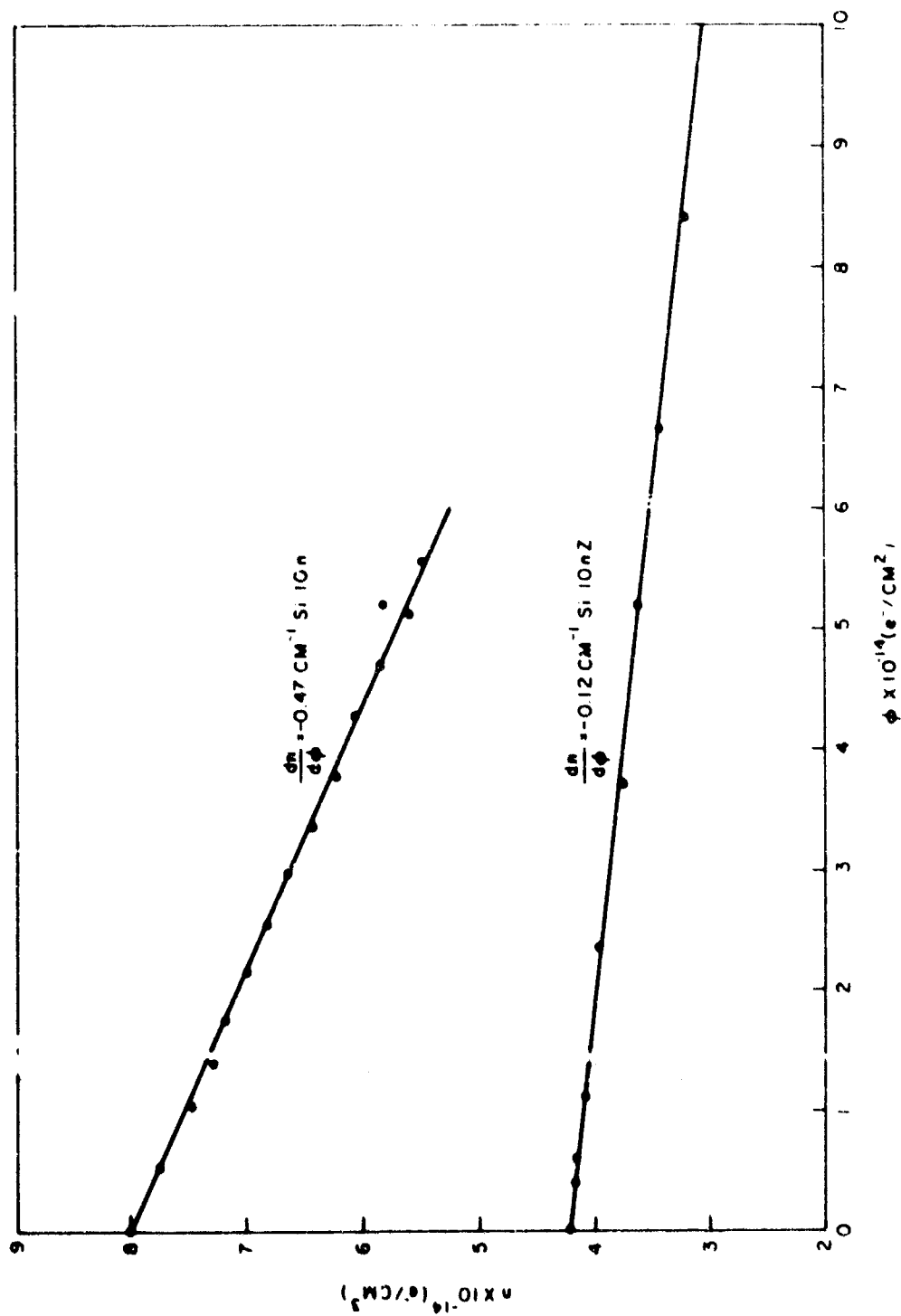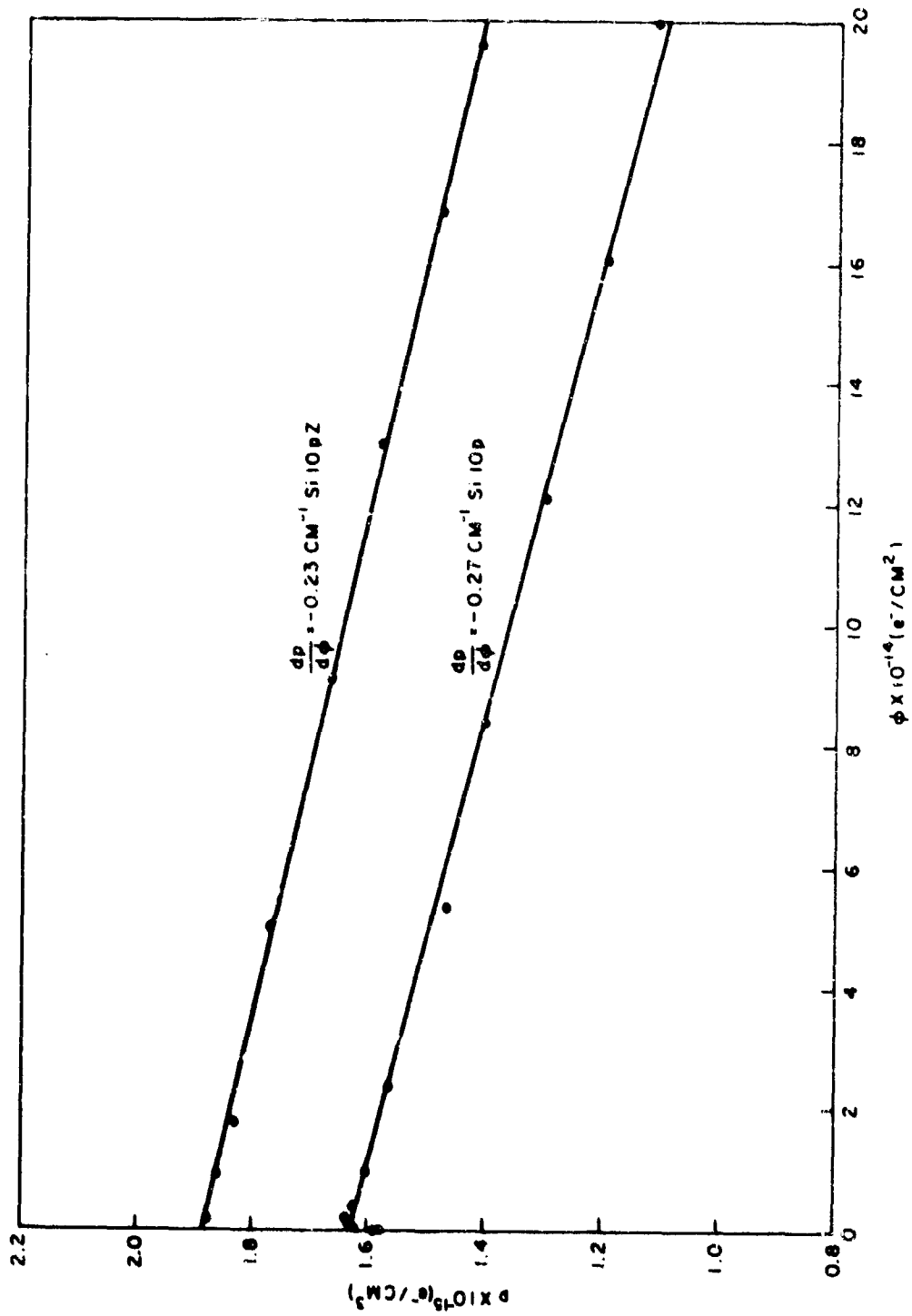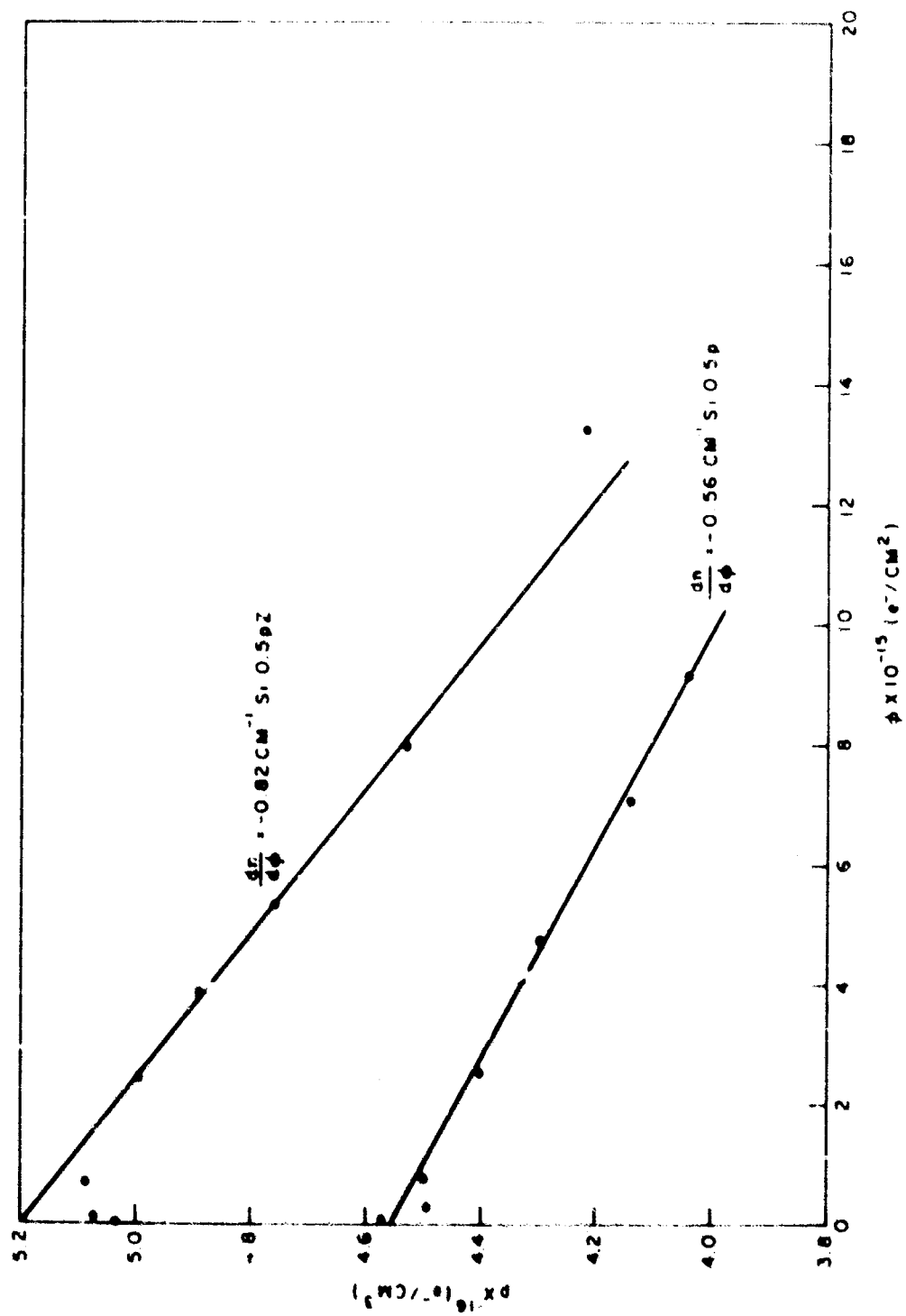
Figure 30   Carrier removal in 0.5-ohm-cm p-type silicon irradiated with 30-MeV electrons
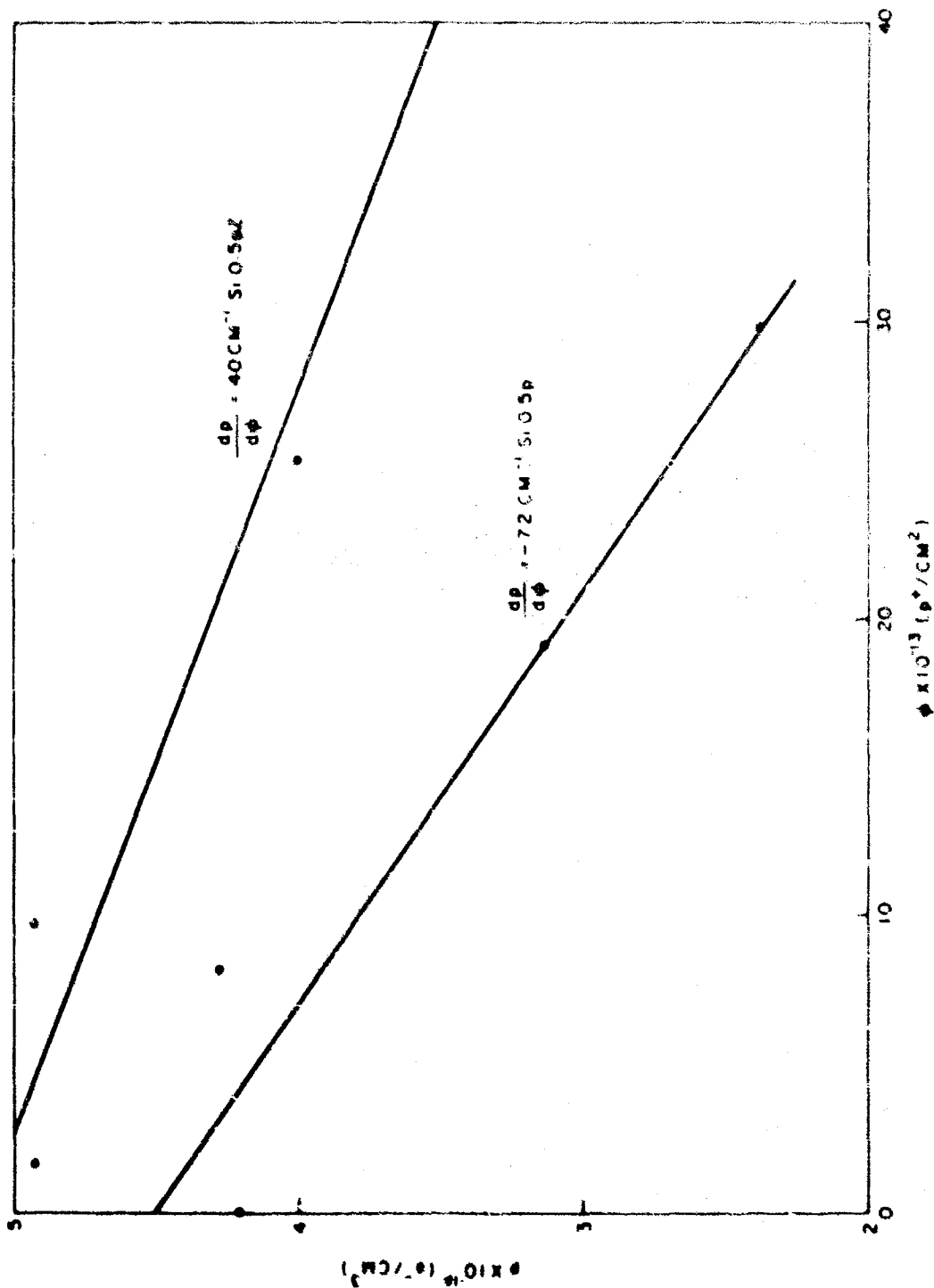
Figure 31. Carrier removal in 0.5-ohm-cm p-type silicon irradiated with 80-MeV protons.
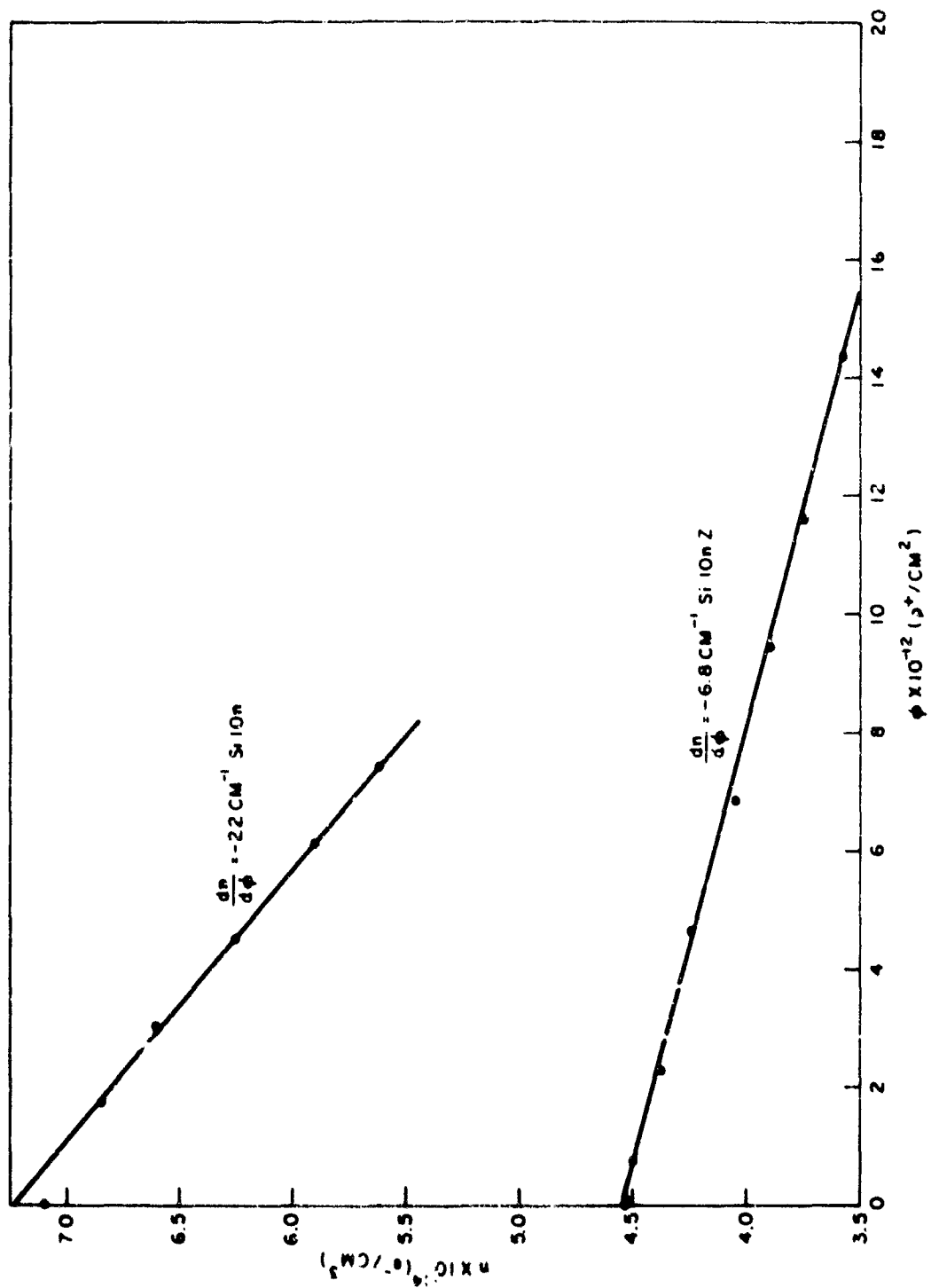
$$\frac{dn}{d\Phi} = .99\,CM^{-1}\ Ge\colon OnZ$$

$\Phi \times 10^{20},\ cm^{-2}$

$n \times 10^{16}\ (e/cm^3)$
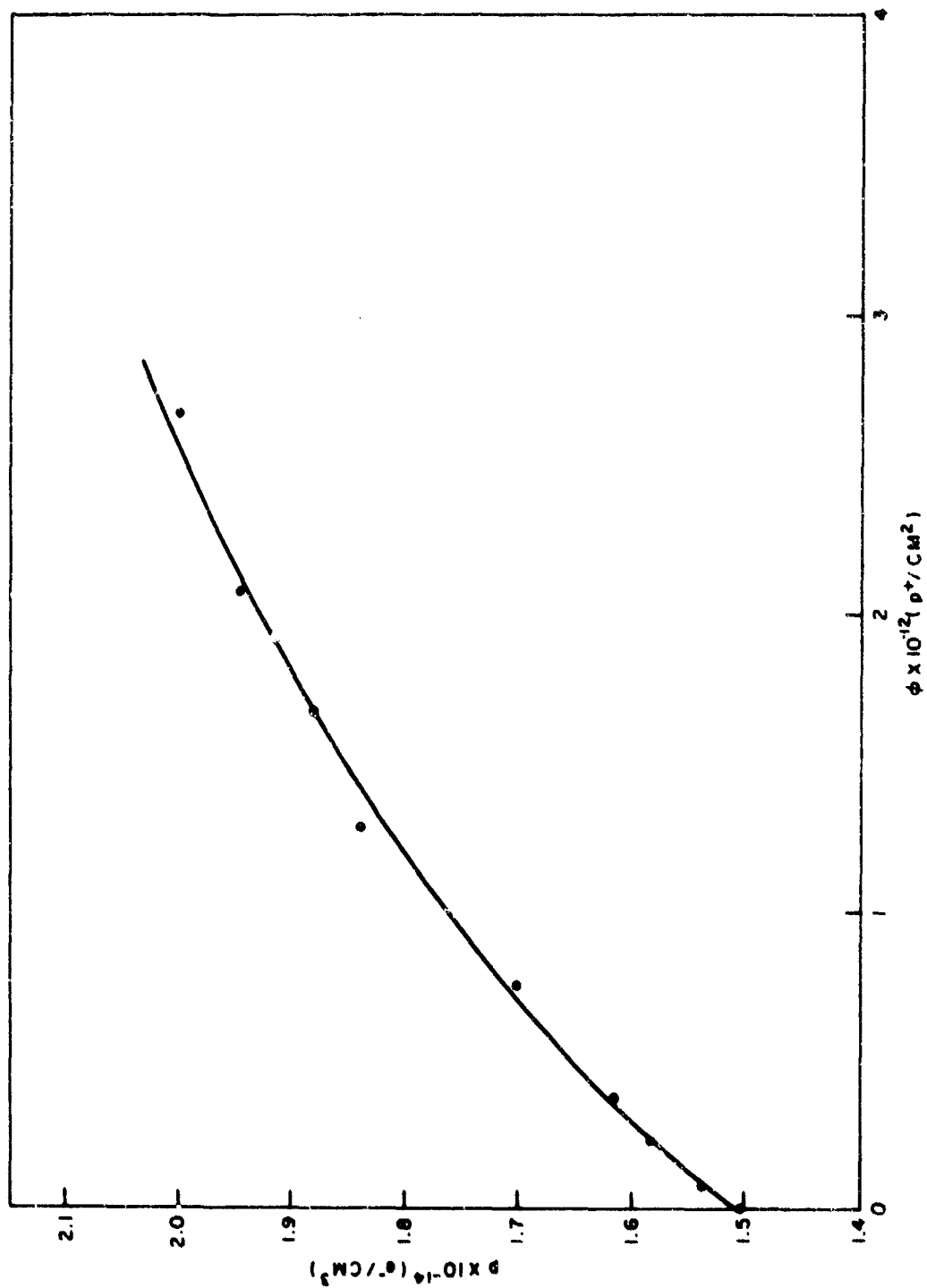
Figure 22

Figure 33. Carrier removal in 10-ohm-cm p-type germanium irradiated with 30-MeV protons

Table III

CARRIER REMOVAL RATES AND INITIAL CARRIER CONCENTRATIONS

Material	Irradiation Energy					
	1.5-MeV electrons	2.3-MeV electrons	5-MeV electrons	30-MeV electrons	30-MeV protons	50-MeV protons
Carrier Removal Rates (in units of carriers/cm^3 per unit flux)						
Si 10n	0.08	0.11	0.17	0.48	22	17
Si 10nZ	0.007	0.015	0.032	0.12	6.8	7.2
Si 10p	0.03	0.05	0.092	0.27	12	7.4
Si 10pZ	0.03	0.05	0.089	0.23	13	9.9
Ge 10nZ	0.38	0.44	0.77	2.4	99	64
Ge 10pZ	0.05	---	0.23	0.4	12	22
Si 0.5n				0.60	28	
Si 0.5nZ				0.45	11	
Si 0.5p				0.56	72	
Si 0.5pZ				0.82	40	
Ge 0.5nZ				3.1	99	
Ge 0.5pZ				0.06		
Initial Carrier Concentrations (in units of carriers/cm^3)						
Si 10n	6.9×10^{14}	6.4×10^{14}	6.3×10^{14}	8.0×10^{14}	7.2×10^{14}	6.8×10^{14}
Si 10nZ	3.6×10^{14}	3.1×10^{14}	3.7×10^{14}	4.2×10^{14}	4.5×10^{14}	3.0×10^{14}
Si 10p	1.6×10^{15}	1.6×10^{15}	1.6×10^{15}	1.6×10^{15}	1.6×10^{15}	1.6×10^{15}
Si 10pZ	1.9×10^{15}	1.9×10^{15}	1.9×10^{15}	1.9×10^{15}	1.9×10^{14}	1.9×10^{15}
Ge 10nZ	3.3×10^{14}	3.9×10^{14}	4.0×10^{15}	3.9×10^{14}	3.6×10^{14}	3.0×10^{14}
Ge 10pZ	2.9×10^{14}	---	2.7×10^{14}	2.3×10^{14}	1.5×10^{14}	1.6×10^{14}
Si 0.5n	---	---	---	0.9×10^{16}	1.2×10^{16}	---
Si 0.5nZ	---	---	---	1.6×10^{16}	2.2×10^{16}	---
Si 0.5p	---	---	---	4.6×10^{16}	4.5×10^{16}	---
Si 0.5pZ	---	---	---	5.2×10^{16}	5.1×10^{16}	---
Ge 0.5nZ	---	---	---	5.8×10^{15}	5.7×10^{15}	---
Ge 0.5pZ	---	---	---	3.9×10^{15}	---	---

4.2 CARRIER LIFETIME IRRADIATIONS

The compilation of the lifetime experimental results is given in Table IV. For the lifetime samples, the specified resistivity tolerance of the boules of ±20% is as good as our dc measurements, taking into consideration the inaccuracies mentioned in Section 4.1. The response of 10-ohm-cm n-type germanium to various electron energy irradiations is given in Fig. 34. This response is typical of the type of results obtained for all samples. The points for the 30-MeV proton irradiation are also shown on an expanded scale. The procedure in these experiments was to measure the lifetime of the samples at the flash X ray before and after the experiments that were not done at General Atomic. In these cases the Strobotac was needed to measure lifetimes during irradiation and the flash X ray served as a check on the Strobotac calibration performed with similar samples at the linear accelerator.

Table IV
LIFETIME DEGRADATION RATES
(in units of 10^{-6} cm^{+2}sec^{-1})

| Material | Irradiation Energy | | | | |
	1.5-MeV electrons	2.3-MeV electrons	5-MeV electrons	30-MeV electrons	30-MeV protons
Si 10n	3	3	7	8	600
Si 10nZ	0.5	1.3	2	3.8	100
Si 10p	0.30	0.45	1.5	5.5	500
Si 10pZ	0.30	0.45	1.5	5.5	500
Ge 10nZ	0.06	0.20	0.30	1.0	27
Ge 10pZ	0.025	0.05	0.06	0.14	18
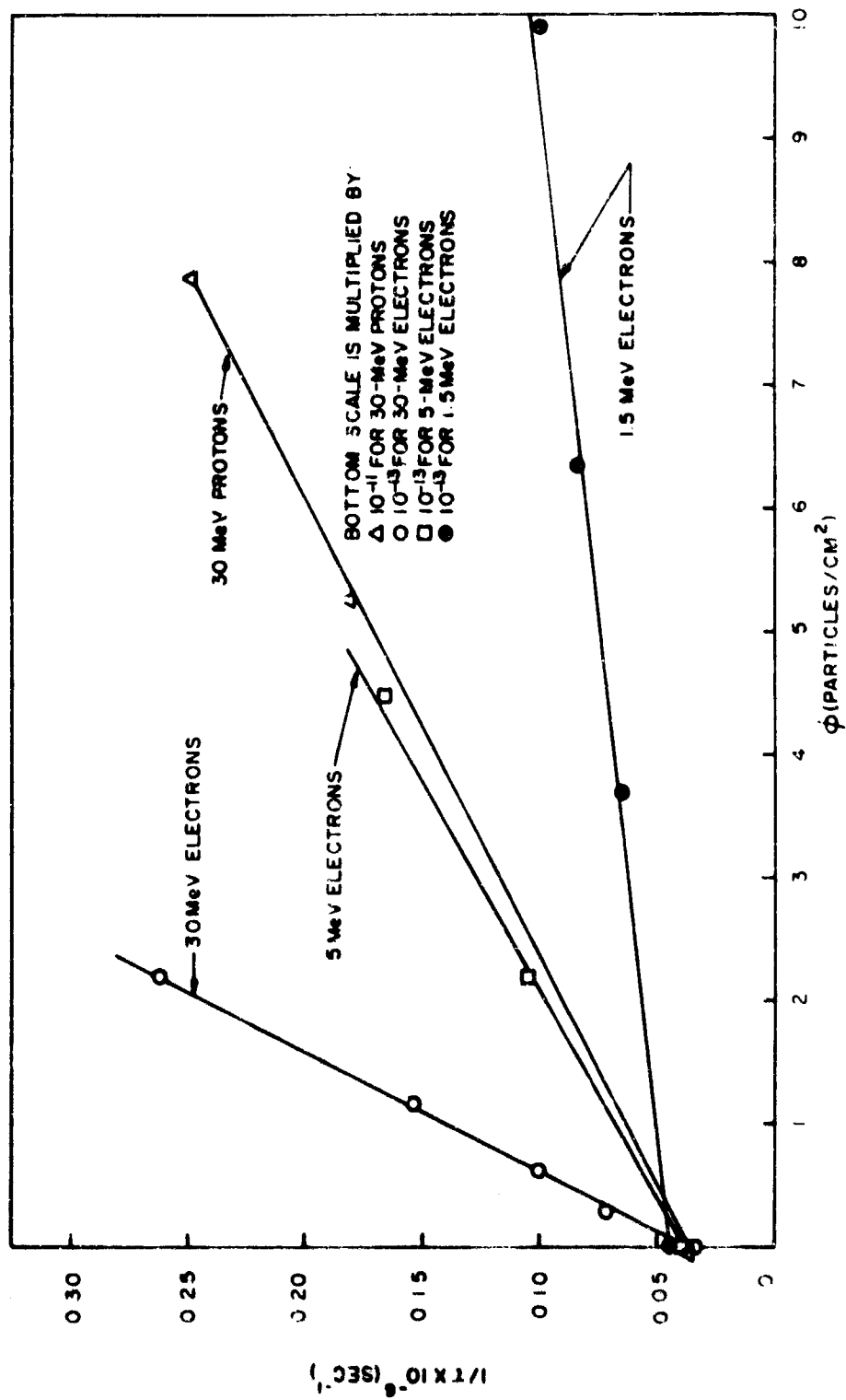
Figure 34. Rate of change of reciprocal lifetime of 10-ohm-cm n-type germanium for various energy radiations

63

4. 3 ANNEALING STUDIES

Annealing experiments were performed after irradiation by holding the sample at 325°, 345°, 367°, 388°, and 400°K successively for 5 min and intermittently cooling to 300°K, at which temperature the measurements were made. For those samples that did show annealing, the results for the Hall samples are shown in Figs. 35 through 39. The fraction of the carriers recovered is defined as $\dfrac{n - n_f}{n_0 - n_f}$, where n_0 is the initial carrier concentration, n_f is the number after the final irradiation, and n is the number after the previous anneal. No annealing was seen for 10-ohm-cm or 0. 5-ohm-cm pulled or floating-zone p-type silicon, 0. 5-ohm-cm floating-zone n-type silicon, or 10-ohm-cm n-type germanium. The annealing was the same within 20 percent for all energy irradiations. For the lifetime samples, with one exception no annealing was observed for any sample, but trapping effects were evident for both p-type silicon samples and the floating-zone refined 10-ohm-cm n-type sample. For p-type silicon, a 30 to 50 percent room temperature anneal was found between the irradiation site and the measurement made at the flash X ray. Thus, for all types of radiations considered here, the annealing data show no evidence of the creation of different types of defects by different irradiating particles.

64
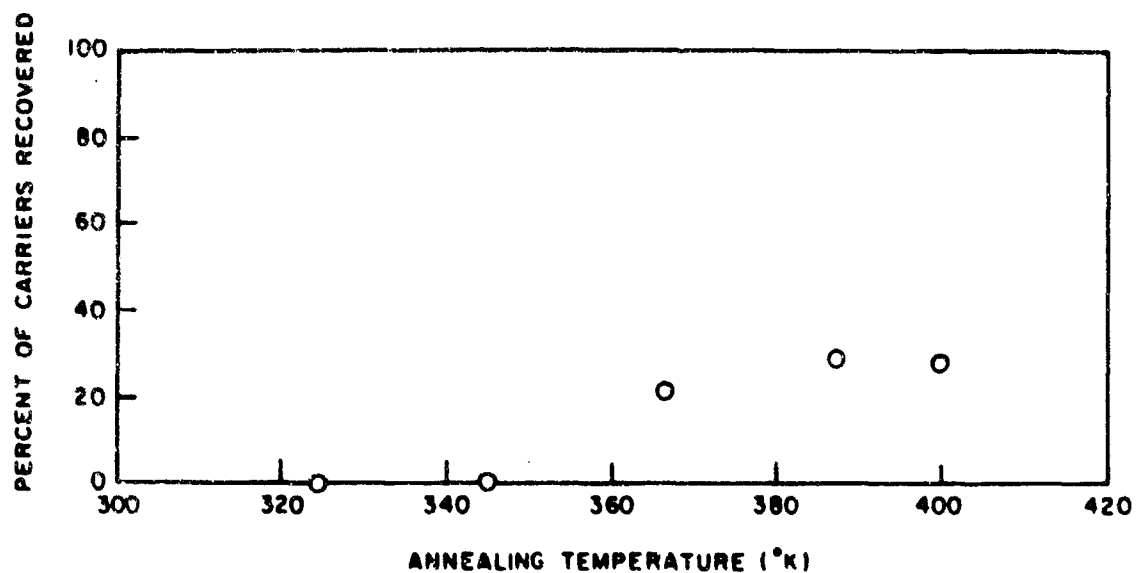
Figure 35. Carrier annealing in 10-ohm-cm n-type, floating-zone, refined silicon
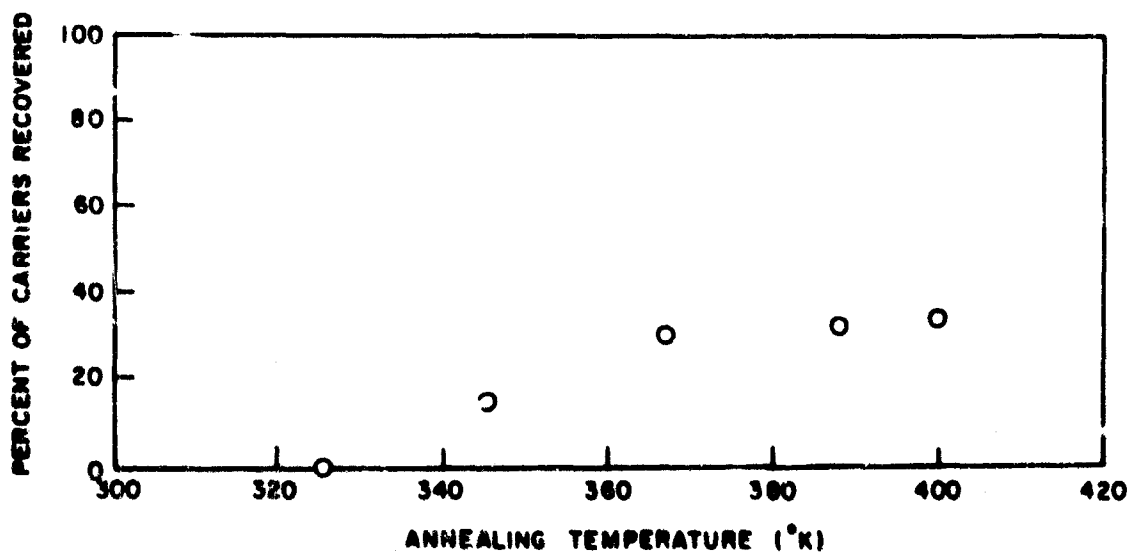
Figure 36. Carrier annealing in 10-ohm-cm n-type, quartz crucible, pulled silicon

65
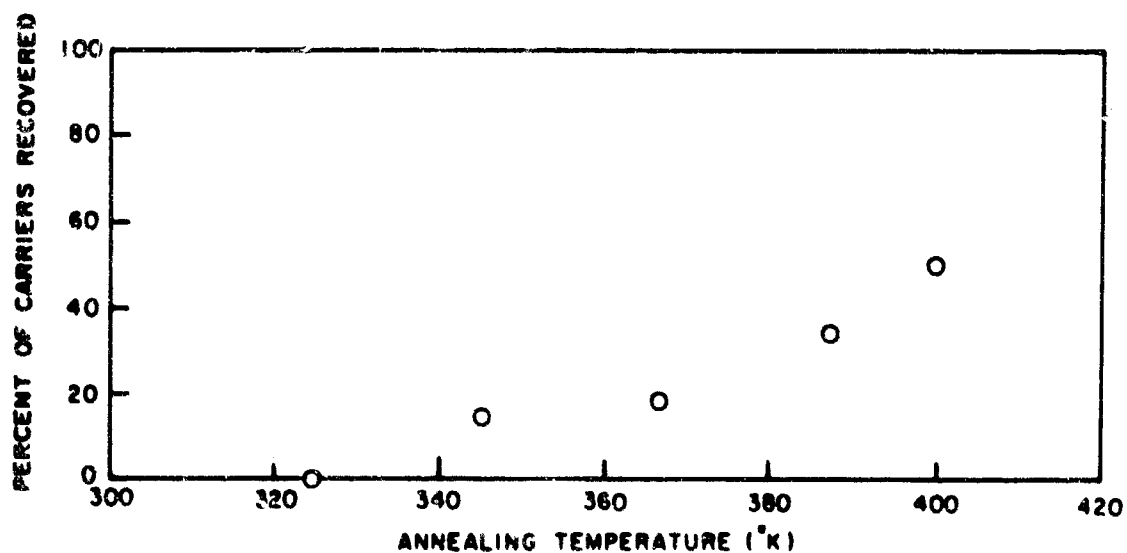
Figure 37. Carrier annealing in 0. 5-ohm-cm n-type, quartz crucible, pulled silicon
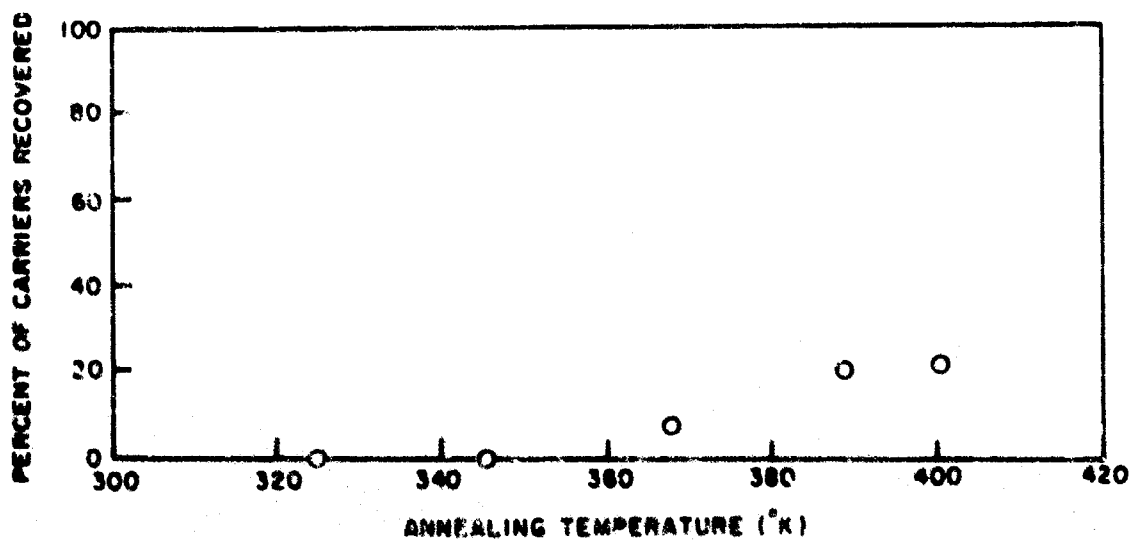
Figure 38. Carrier annealing in 0. 5-ohm-cm n-type germanium
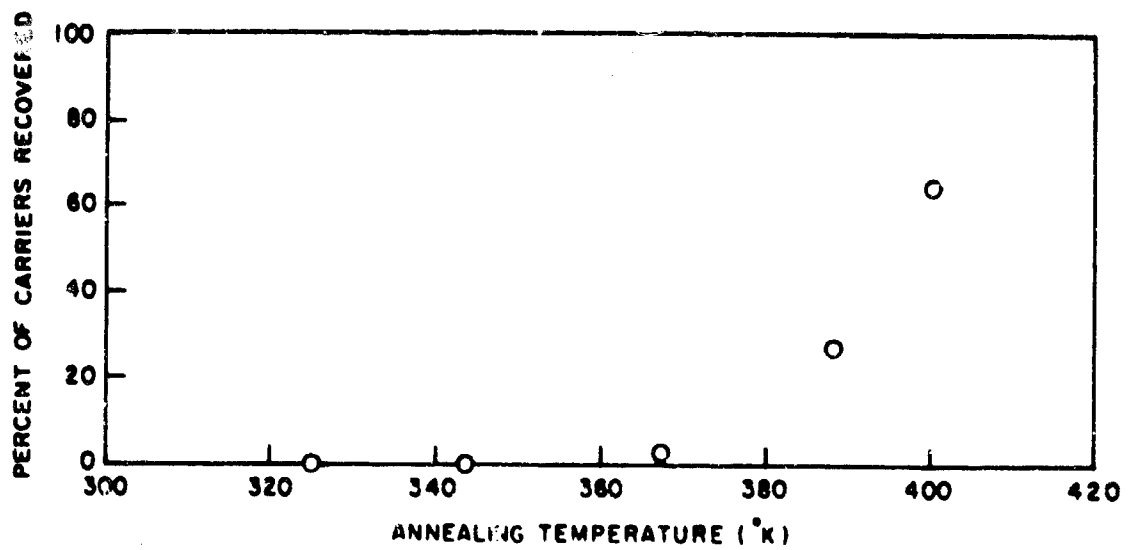
Figure 39. Carrier annealing in 10-ohm-cm p-type germanium

SECTION V

DISCUSSION

It is now possible to compare the experimental data with theory.
Since neutron irradiations were not included in the experimental program,
it is not possible to perform a direct check on the best simulation predic-
tion presented in Section 2.8. Instead, a comparison between experiment
and a correlation with total displaced atoms can be examined. It is re-
cognized that this correlation may be inaccurate since the higher-energy
and higher-mass particles produce a larger fraction of the displacements
via more energetic recoil atoms. This comparison is presented in
Table V as ratios between the rate of introduction of defects relative to
the introduction rate in the same material by 30-MeV electrons.

Another more instructive comparison is achieved by calculating the
property change per unannealed displaced atom calculated as in Section II.
These data are summarized in Table VI.

The radiation response presented in Table VI is discussed in more
detail below.

5.1 n-TYPE SILICON

The lifetime degradation data for n-type silicon follow the theory
fairly well for the electron irradiations from 1.5 to 30-MeV, whereas the
30-MeV proton data show a relative increase in defect production over theory.
The data for both pulled and floating-zone material can be expected to show
more scatter than similar irradiations with other materials because of a
6-μsec trapping time in the floating-zone material that makes an accurate
measurement of the low injection level difficult and the unexpectedly low
unirradiated bulk lifetime of the pulled material. The latter was less
than 1 μsec, which is an order of magnitude less than is to be expected for

Table V
COMPARISON OF DEFECT INTRODUCTION RATES

Material[a]	Measure-ments[b]	Defect Introduction Rate Relative to 30-MeV Electrons				
		1.5-MeV e⁻	2.3-MeV e⁻	5-MeV e⁻	30-MeV p⁺	50-MeV p⁺
Si	Theory	0.31	0.40	0.58	27	18
Si 10N	H	0.17	0.23	0.36	46	35
	τ	0.38	0.38	0.88	75	
Si 10NZ	H	0.06	0.13	0.27	58	60
	τ	0.13	0.34	0.53	26	
Si 10P	H	0.11	0.19	0.34	46	27
	τ	0.054	0.08	0.27	91	
Si 10PZ	H	0.13	0.21	0.38	55	43
	τ	0.054	0.08	0.27	91	
Si 0.5N	H				47	
Si 0.5NZ	H				24	
Si 0.5P	H				130	
Si 0.5PZ	H				49	
Ge	Theory	0.18	0.27	0.46	20	14
Ge 10NZ	H	0.16	0.18	0.32	41	27
	τ	0.06	0.20	0.30	27	
Ge 10PZ	H	0.13		0.57	30	54
	τ	0.18	0.36	0.43	13	
Ge 0.5NZ	H				32	

[a]Number is resistivity, in ohm-cm, N and P are conductivity type, Z represents quartz-crucible-grown crystals; absence of Z implies floating-zone refined crystals.

[b]H = carrier removal rate from Hall coefficient,

τ = rate of change of reciprocal of carrier lifetime.

Table VI

MEASURED PROPERTY CHANGE PER CALCULATED UNANNEALED DISPLACED ATOM

Materials	Measurement*	1.5 MeV e⁻	2.3 MeV e⁻	5 MeV e⁻	30 MeV e⁻	30 MeV p*	50 MeV p⁻
Si 10N	H	0.045	0.046	0.050	0.081	0.14	0.15
	τ	1.6	1.3	2.0	1.4	3.8	
Si 10NZ	H	0.0039	0.0063	0.0094	0.020	0.043	0.062
	τ	0.3	0.5	0.6	0.6	0.6	
Si 10P	H	0.017	0.021	0.027	0.046	0.076	0.063
	τ	0.17	0.19	0.44	0.93	3.2	
Si 10PZ	H	0.017	0.021	0.026	0.039	0.082	0.085
	τ	0.17	0.19	0.44	0.93	3.2	
Si 0.5N	H				0.10	0.18	
Si 0.5NZ	H				0.076	0.070	
Si 0.5P	H				0.095	0.46	
Si 0.5PZ	H				0.14	0.25	
Ge 10NZ	H	0.25	0.20	0.21	0.29	0.05	0.55
	τ	0.04	0.09	0.08	0.13	0.17	
Ge 10PZ	H	0.03		0.06	0.05	0.07	0.2
	τ	0.017	0.023	0.016	0.017	0.11	
Ge 0.5NZ	H				0.4	0.7	
Ge 0.5PZ	H				0.007		

See Table V for explanation of symbols.

this material. This not only affects the accuracy of the data (e.g., room temperature annealing between the irradiation site and post-irradiation measurements at the flash X ray could go unnoticed owing to the difficulty of measuring such a short lifetime with the light source) but also the applicability to other materials of this type, since a different defect than is usual may be producing the irradiation response.

These data may be compared with those from damage to p on n silicon solar cells due to protons[18] and due to electrons.[19,20] The solar-cell damage measured is the minority carrier diffusion length, which is comparable to the minority carrier lifetime. The electron irradiations, which covered bombarding energies from 0.4 to 40 MeV, showed substantial agreement with simple theory over the range from 1.5 to 30 MeV. However, the proton damage measured with 17- to 130-MeV particles showed a slowly falling damage rate from 17 to 50 MeV that cannot be totally ascribed to rising contributions from either nuclear elastic scattering or star production. Above 50 MeV, the damage rate assumes the 1/E character expected from Rutherford scattering. The floating-zone data are in agreement with this, showing that recoils from 30-MeV protons have twice the predicted effectiveness in producing damage than recoils from 1.5 to 30-MeV electrons. Also, lifetime degradation rates measured with neutrons from a TRIGA reactor[21] give a property change per unannealed displaced atom of 8, using half the calculated neutron cross section because the spectrum used in the irradiations was softer than the one calculated in Section II. When the above data are compared with the theory presented in Section II, they are consistent with an assumption that primary recoils of the order of 10^{-5} eV are approximately four times more efficient than predicted in producing damage in a room-temperature irradiation than recoils an order of magnitude lower in energy.

For the floating-zone material, the radiation response of the Hall coefficient seems to follow that of the lifetime up to the 50-MeV proton irradiation, where the increase in damage over that expected levels off instead of further increasing as do the data of Rosenzweig on lifetime.

71

The pulled material exhibits a gradual increase over theoretical damage as the irradiating electron energy is raised, but otherwise follows the behavior of the floating-zone material. Carrier-removal experiments with neutron irradiations have been done by Stein[22] as well as by Curtis[21] but their results are in disagreement by factors of 2 to 4, with Stein's removal rates being the higher. Curtis's results give a property change per unannealed displaced atom of 0.03 and 0.025 for floating-zone and pulled silicon, respectively, which are much lower than expected in the light of the proton data and the apparent agreement with our lifetime data.

5.2 p-TYPE SILICON

No significant differences between pulled and floating-zone p-type silicon were observed in either lifetime or Hall damage rates in any irradiation.

Lifetime damage may again be compared with damage to n on p silicon solar cells in Refs. 18, 19, and 21. The electron irradiations from 0.4 to 40 MeV show results much like those derived here, with the damage rising with increasing bombarding energy much faster than is calculated. In fact Carter and Downing fit their data to the square of the displacement cross section. Our electron irradiations fit such a curve quite well, but the 30-MeV proton irradiations show a smaller increase as do the neutron data of Curtis, with a property change per unannealed displaced atom of 7×10^{-8} cm^2 sec^{-1}. The proton data of Rosenzweig from 1.35 to 130 MeV shows similar behavior. Below 8 MeV, the damage rate rises as $1/E$ in accordance with Rutherford scattering, but above 10 MeV, the damage rate falls only slightly up to 50 MeV, where it resumes an approximate $1/E$ behavior again. As with n-type silicon, calculations cannot account for this behavior, even when all the recoil energy is assumed to go into producing displacements, which is an unlikely condition. With a more realistic division of energy between displacements and ionization, such as imposing a limit of about 10^5 eV above which recoils are

72

assumed to lose all their energy by ionization, the divergence from the experimental curve is much greater and probably cannot be ascribed to star production.

The Hall data follow the same characteristics as the lifetime data, but there is a slower increase in damage efficiency as the energy rises. This behavior is also indicated in data on carrier removal in 15- to 150-ohm-cm p-type silicon.[19] The 30- and 50-MeV protons seem to follow theoretical predictions in producing Hall damage in p-type silicon. Curtis's results are, as before with n-type silicon, lower than expected, with a property change per unannealed displaced atom of 0.03.

Thus, in both n- and p-type silicon, the higher-energy primary recoil atoms seem to have an effect that scales faster than the total number of displaced atoms they produce. The magnitude depends on the material and indeed even on the type of damage.

5.3 GERMANIUM

Lifetime damage in n- and p-type germanium is in an essentially constant ratio to that calculated for all irradiations, except for a small rise in n-type germanium and a large rise in p-type germanium with 30-MeV protons.

Hall irradiations on n-type germanium are in agreement with theory for electrons, but again protons produce damage more efficiently. P-type germanium is a special case as the removal rates change with carrier concentration and previous irradiation history, which makes a comparison between irradiations hazardous.

Again, with germanium as with silicon, it seems that the high-energy recoils have an effect on the damage that rises more rapidly than the number of displaced atoms.

The lack of differences in the annealing behavior only indicates that the particular defects which anneal in the temperature range 300°K to

73

400°K are formed proportionately by all of the irradiating particles. This observation makes no inference on the correlation between those other defects which did not anneal in this temperature range.

SECTION VI

CONCLUSIONS

From the experiments performed, it was found that the defect introduction rate rises faster with rising irradiating energies than the number of unannealed displaced atoms. It is apparent that the effect of displaced atoms on both lifetime and carrier concentration is greater if the atoms are produced by higher-energy recoils. This effect is magnified further if it is noted that more than half of the displacements produced by protons are associated with recoil atoms having the same energy spectrum as those produced by 30-MeV electrons. Thus, the apparent increase in over-all effectiveness of the protons must be attributed to less than half of the damage. Therefore, an apparent increase of damage per displaced atom of a factor of 2 to 3 must represent an increased effectiveness of displaced atoms produced by the higher-energy recoil atoms of a factor of 3 to 5. Hence, it is predicted that the property change per unannealed displaced atoms should be even greater for neutrons than for the highest energy protons used, and indeed this is the case for lifetime damage in similar materials irradiated by other workers.[21, 22]

For Hall damage, the situation is less clear as there are two pieces of conflicting data, but if the higher rates of Stein's data[22] are correct, then the above conclusion is upheld.

The difficulty in interpreting this apparent high effectiveness of primary recoils in the range of 100 keV in producing damage is heightened by an understanding of the process by which a recoil atom loses its energy.[1] The majority of collisions the primary recoil suffers in slowing to an energy less than 10 keV (where it seems not to produce excessive damage) involve small energy transfers and any displacement

75

clusters produced are quite far apart and are in no essential way different from those produced by a less energetic recoil. However, calculations show that a 1-keV recoil produces displaced atoms in its track about 4 lattice constants apart, which is within the interaction distance for the displacements (4 to 6 lattice constants), whereas a 100-keV recoil along the initial portion of its track produces displacements about 15 lattice constants apart along with substantially more ionization. This combination of distantly spaced displacements in an ionized region may well produce secondary defects in different proportions from the displaced atoms from lower energy recoils which find themselves fairly closely spaced in a neutral region.

It would seem that this behavior would be different for different materials, and for different defects controlling the irradiation response. This does seem to be the case as the varying results between material and parameter measured show. Also, impurities or defects not involved in the defect directly responsible for the radiation response may affect or even control the difference in the high-energy recoil damage efficiency.

Thus, while it is possible that the above data can be used for purposes of proton simulation with electrons, extreme care must be taken to ensure that the defect controlling the radiation response is the same as that measured here and that no impurity is present that would affect the damage rate of the high-energy recoils present with protons. A simulation with a better chance of success would be an admixture of electrons and reactor neutrons, as described in the theoretical portion of this report.

REFERENCES

1. van Lint, V. A. J., and M. E. Wyatt, Range of Recoil Atoms, Aeronautical Research Laboratories, Report ARL-62-398, Contract AF33(616)-6795.

2. Lindhard, J., V. Nielsen, M. Scharff, and P. V. Thomsen, Kgl. Danske Videnskab. Selskab, Mat. -fys. Medd. 33 No. 10 (1963).

3. Seitz, F., and J. S. Koehler, Solid State Physics, Vol. 2, Academic Press, New York, 1956, p. 307.

4. Perey, F. G., Phys. Rev. 131, 745 (1963).

5. Perey, F. G., and B. Buck, Nuclear Phys. 32, 353 (1962).

6. Buck, B., Phys. Rev. 130, 712 (1963).

7. Woods, R. D., Phys. Rev. 106, 793 (1957).

8. Kinsey, B. B., and T. Stone, Phys. Rev. 103, 975 (1956).

9. Glassgold, A. E., and P. J. Kellogg, Phys. Rev. 107, 1372 (1957).

10. Fulmer, C. B., Phys. Rev. 125, 631 (1962).

11. Glassgold, A. E., and P. J. Kellogg, Phys. Rev. 109, 1291 (1958).

12. Yamabe, S., M. Takeda, M. Kondo, S. Kato, T. Yamazaki, N. Takahashi, N. Kawai, and R. Chiba, J. Phys. Soc. Japan 17, 729 (1962).

13. Brussel, M. K., and J. H. Williams, Phys. Rev. 114, 525 (1959).

14. McKinley, W. A., and H. Feshbach, Phys. Rev. 74, 1759 (1948).

15. Larsen, J. E., E. G. Wikner, and D. K. Nichols, Displacement
    Radiation Effects, Appendix II, Final Report on Contract DA-49-186-
    ORD-984, General Atomic, Report GA-5088, 1964.

16. Goldberg, M. D., V. M. May, and J. R. Stehn, Brookhaven National
    Laboratory, Report BNL-400, 1962.

17. Hughes, D. J., and R. B. Schwartz, Neutron Cross Sections, Brook-
    haven National Laboratory, Report BNL-325, 1962.

18. Rosenzweig, W., F. M. Smits, and W. L. Brown, J. Appl. Phys.
    35, 2707 (1964).

19. Carter, J. R., and R. G. Downing, Charged-particle Radiation Dam-
    age in Semiconductors. XI: Effects of Low-energy Protons and High-
    energy Electrons on Silicon, Interim Technical Final Report on Contract
    NAS5-3805, TRW Space Technology Laboratories, Report 4161-6012-
    RU-000, May 1965.

20. Charged-particle Radiation Damage in Semiconductors. X: The
    Energy Dependence of Electron Damage in Silicon, Contract NAS5-
    3805, TRW Space Technology Laboratories, Report 4161-6004-KU-000,
    September 1964.

21. Curtis, O. L., Jr., R. F. Bass, and C. A. Germano, Impurity
    Effects in Neutron-irradiated Silicon and Germanium, Harry Diamond
    Laboratories, Report 235-1 (NARD-65-20R), November 1965.

22. Stein, H. J., Introduction Rate of Electrically Active Defects in Sili-
    con by Nuclear Radiation, Sandia Corporation Reprint SC-R-64-193,
    1964.

DOCUMENT CONTROL DATA - R&D

(Security classification of title, body of abstract and indexing annotation must be entered when the overall report is classified)

1. ORIGINATING ACTIVITY (Corporate author)	2a. REPORT SECURITY CLASSIFICATION
Special Nuclear Effects Laboratory General Atomic Division General Dynamics Corporation, San Diego, Calif.	Unclassified
	2b. GROUP

3. REPORT TITLE

PROTON CORRELATION STUDIES

4. DESCRIPTIVE NOTES (Type of report and inclusive dates)

Final Report (1 July 1964 through 31 January 1966)

5. AUTHOR(S) (Last name, first name, initial)

M. E. Wyatt
V. A. J. van Lint.
E. G. Wikner

6. REPORT DATE	7a. TOTAL NO. OF PAGES	7b. NO. OF REFS
April 1966	86	22

8a. CONTRACT OR GRANT NO. AF 33(615)-1715	9a. ORIGINATOR'S REPORT NUMBER(S)
b. PROJECT NO.	GA-6953
c.	9b. OTHER REPORT NO(S) (Any other numbers that may be assigned this report)
d.	AFML-TR-66-77

10. AVAILABILITY/LIMITATION NOTICES

This document is subject to special export controls and each transmittal to foreign governments or foreign nationals may be made only with prior approval of AFML (MAYT), WPAFB, Ohio 45433.

11. SUPPLEMENTARY NOTES	12. SPONSORING MILITARY ACTIVITY
	Air Force Materials Laboratory Research and Technology Division Wright-Patterson Air Force Base, Ohio

13. ABSTRACT

The radiation effects of high-energy protons and electrons on germanium and silicon have been studied. The influence of the damage on the Hall effect and minority carrier lifetime produced by 1.5-, 2.3, 5-, and 30-MeV electrons is compared with that produced by 30- and 50-MeV protons. The experimental results are directly compared with the theoretical predictions of the damage. It is concluded that the higher-energy recoils resulting from the proton irradiations are more effective in producing damage than those resulting from the electron irradiations, based on the predictions of the total number of the defects that different types of particles are expected to produce. The reason for this may be that the higher-energy recoils produce displacements which are separated farther and thereby influence the measured properties in a different manner.

Complexities in correlating proton and electron damage which arise from the influence of impurities and defect motion during irradiation are discussed. A proton simulation based on an admixture of electrons and reactor neutrons is discussed theoretically.

DD FORM 1 JAN 64 1473

14. KEY WORDS	LINK A		LINK B		LINK C	
	ROLE	WT	ROLE	WT	ROLE	WT
Proton and Electron damage in n- and p-type Ge and Si						
Experimental results						
Theoretical correlation study						
Theory of neutron damage						

INSTRUCTIONS

1. ORIGINATING ACTIVITY: Enter the name and address of the contractor, subcontractor, grantee, Department of Defense activity or other organization (*corporate author*) issuing the report.

2a. REPORT SECURITY CLASSIFICATION: Enter the overall security classification of the report. Indicate whether "Restricted Date" is included. Marking is to be in accordance with appropriate security regulations.

2b. GROUP: Automatic downgrading is specified in DoD Directive 5200.10 and Armed Forces Industrial Manual. Enter the group number. Also, when applicable, show that optional markings have been used for Group 3 and Group 4 as authorized.

3. REPORT TITLE: Enter the complete report title in all capital letters. Titles in all cases should be unclassified. If a meaningful title cannot be selected without classification, show title classification in all capitals in parenthesis immediately following the title.

4. DESCRIPTIVE NOTES: If appropriate, enter the type of report, e.g., interim, progress, summary, annual, or final. Give the inclusive dates when a specific reporting period is covered.

5. AUTHOR(S): Enter the name(s) of author(s) as shown on or in the report. Enter last name, first name, middle initial. If military, show rank and branch of service. The name of the principal author is an absolute minimum requirement.

6. REPORT DATE: Enter the date of the report as day, month, year; or month, year. If more than one date appears on the report, use date of publication.

7a. TOTAL NUMBER OF PAGES: The total page count should follow normal pagination procedures, i.e., enter the number of pages containing information.

7b. NUMBER OF REFERENCES: Enter the total number of references cited in the report.

8a. CONTRACT OR GRANT NUMBER: If appropriate, enter the applicable number of the contract or grant under which the report was written.

8b, 8c, & 8d. PROJECT NUMBER: Enter the appropriate military department identification, such as project number, subproject number, system numbers, task number, etc.

9a. ORIGINATOR'S REPORT NUMBER(S): Enter the official report number by which the document will be identified and controlled by the originating activity. This number must be unique to this report.

9b. OTHER REPORT NUMBER(S): If the report has been assigned any other report numbers (*either by the originator or by the sponsor*), also enter this number(s).

10. AVAILABILITY/LIMITATION NOTICES: Enter any limitations on further dissemination of the report, other than those imposed by security classification, using standard statements such as:

   (1) "Qualified requesters may obtain copies of this report from DDC."

   (2) "Foreign announcement and dissemination of this report by DDC is not authorized."

   (3) "U. S. Government agencies may obtain copies of this report directly from DDC. Other qualified DDC users shall request through

     _____."

   (4) "U. S. military agencies may obtain copies of this report directly from DDC. Other qualified users shall request through

     _____."

   (5) "All distribution of this report is controlled. Qualified DDC users shall request through

     _____."

If the report has been furnished to the Office of Technical Services, Department of Commerce, for sale to the public, indicate this fact and enter the price, if known.

11. SUPPLEMENTARY NOTES: Use for additional explanatory notes.

12. SPONSORING MILITARY ACTIVITY: Enter the name of the departmental project office or laboratory sponsoring (*paying for*) the research and development. Include address.

13. ABSTRACT: Enter an abstract giving a brief and factual summary of the document indicative of the report, even though it may also appear elsewhere in the body of the technical report. If additional space is required, a continuation sheet shall be attached.

It is highly desirable that the abstract of classified reports be unclassified. Each paragraph of the abstract shall end with an indication of the military security classification of the information in the paragraph, represented as (TS), (S), (C), or (U).

There is no limitation on the length of the abstract. However, the suggested length is from 150 to 225 words.

14. KEY WORDS: Key words are technically meaningful terms or short phrases that characterize a report and may be used as index entries for cataloging the report. Key words must be selected so that no security classification is required. Identifiers, such as equipment model designation, trade name, military project code name, geographic location, may be used as key words but will be followed by an indication of technical context. The assignment of links, rules, and weights is optional.

GPO 886-551